Article

Cell
PRESS

AAK1 Identified as an Inhibitor of Neuregulin-1/ErbB4-Dependent Neurotrophic Factor Signaling Using Integrative Chemical Genomics and Proteomics

Letian Kuai,[1,6] Shao-En Ong,[2,7] Jon M. Madison,[1] Xiang Wang,[2,8] Jeremy R. Duvall,[2] Timothy A. Lewis,[2]
Catherine J. Luce,[1] Sean D. Conner,[3] David A. Pearlman,[1] John L. Wood,[4] Stuart L. Schreiber,[2] Steven A. Carr,[2]
Edward M. Scolnick,[1] and Stephen J. Haggarty[1,5,*]
[1]Stanley Center for Psychiatric Research
[2]Broad Institute of Harvard and MIT
7 Cambridge Center, Cambridge, MA 02142, USA
[3]Department of Genetics, Cell Biology and Development, University of Minnesota, 6-160 Jackson Hall, 321 Church Street SE,
Minneapolis, MN 55455, USA
[4]Department of Chemistry, Colorado State University, Fort Collins, CO 80523, USA
[5]Center for Human Genetic Research, Massachusetts General Hospital, Department of Neurology, Harvard Medical School,
185 Cambridge Street, Boston, MA 02114, USA
[6]Present Address: GlaxoSmithKline, 830 Winter Street, Waltham, MA 02142, USA
[7]Present Address: Department of Pharmacology, University of Washington, School of Medicine, Seattle, WA 98195-7280, USA
[8]Present Address: Department of Chemistry and Biochemistry, University of Colorado, Boulder, CO 80309, USA
*Correspondence: haggarty@chgr.mgh.harvard.edu
DOI 10.1016/j.chembiol.2011.03.017

SUMMARY

Target identification remains challenging for the field of chemical biology. We describe an integrative chemical genomic and proteomic approach combining the use of differentially active analogs of small molecule probes with stable isotope labeling by amino acids in cell culture-mediated affinity enrichment, followed by subsequent testing of candidate targets using RNA interference-mediated gene silencing. We applied this approach to characterizing the natural product K252a and its ability to potentiate neuregulin-1 (Nrg1)/ErbB4 (v-erb-a erythroblastic leukemia viral oncogene homolog 4)-dependent neurotrophic factor signaling and neuritogenesis. We show that AAK1 (adaptor-associated kinase 1) is a relevant target of K252a, and that the loss of AAK1 alters ErbB4 trafficking and expression levels, providing evidence for a previously unrecognized role for AAK1 in Nrg1-mediated neurotrophic factor signaling. Similar strategies should lead to the discovery of novel targets for therapeutic development.

INTRODUCTION

Chemical genomics employs small molecule probes to help elucidate the relationship between genes and biological functions. A forward chemical-genetic study typically begins by perturbing a biological system with a panel of small molecules followed by identification of the relevant targets of the compound that generates the phenotype of interest (Stockwell, 2000). However, small molecules can have variable specificity such

that identifying the full complement of biologically relevant protein, or other molecular targets, often presents a formidable challenge. Traditional target identification strategies typically employ affinity-based isolation, gel visualization, and sequencing, which is often limited and biased to a high-affinity protein-probe association and the isolation of highly abundant proteins. Recently, the application of stable isotope labeling by amino acids in cell culture (SILAC)-based quantitative mass spectrometry methodology using isotope-labeled cell lysates in pull-down experiments has been shown to provide a sensitive and unbiased means to determine cellular-binding partners of small molecule probes (Ong et al., 2002, 2009). However, although powerful, the use of this methodology still requires additional strategies to reveal functionally important binding interactions, which often remains the rate-limiting step in the "target identification" challenge.

We have recently focused on the identification and development of chemical probes and miniaturized imaging assays to understand neuregulin-1 (Nrg1)/v-erb-a erythroblastic leukemia viral oncogene homolog 4 (ErbB4) signaling (Kuai et al., 2010). Nrg1 belongs to a family of four growth factors (Nrg1–4) that each contain an epidermal growth factor (EGF)-like domain and play a multitude of roles ranging from the regulation of cell proliferation to synaptic plasticity. In humans the *NRG1* gene produces at least 31 isoforms in 6 types of protein (I–VI) by alternative splicing and proteolytic cleavage (Falls, 2003). It is commonly believed that Nrg1 serves as a trophic factor that signals by activating the ErbB receptor family (Bublil and Yarden, 2007), of which ErbB4 is the fourth member. Although all the ErbB tyrosine kinase receptors are potentially activated by Nrg1, only ErbB3 and ErbB4 have been shown to directly bind Nrg1. ErbB2 and ErbB1 (epidermal growth factor receptor [EGFR]) are instead activated as coreceptors (Tzahar et al., 1994). In addition, the kinase activity of ErbB3 is impaired (Guy et al., 1994), and ErbB4 is the only receptor that specifically

binds to Nrg1 and becomes autophosphorylated. Activation of ErbB receptors subsequently activates many downstream signaling pathways, including Raf-MEK-ERK and PI3K-AKT signaling, which lead to a variety of cellular responses. In neuronal development the Nrg1-ErbB4 signaling has been shown to participate in crucial processes, such as neuronal migration, axon guidance, and synapse formation (Mei and Xiong, 2008). In mature neurons, Nrg1-ErbB4 signaling is also implicated in synaptic plasticity and neuronal survival (Mei and Xiong, 2008). In both cases we lack a full understanding of the molecular mechanisms through which Nrg1-ErbB4 signaling is regulated and how alterations of this signaling impacts cellular physiology.

To identify small molecule modulators of Nrg1-ErbB4 signaling that would enable a better understanding of the underlying molecular mechanisms, we previously established an image-based, live cell, high throughput screening system utilizing a PC12 cell line stably expressing human ErbB4 along with green fluorescent protein (GFP) for ease of visualization (Kuai et al., 2010). Native PC12 cells express the receptor for nerve growth factor (NGF), TrkA, but do not express ErbB4. By expressing exogenous ErbB4, the PC12-ErbB4-GFP cells are able to respond to Nrg1 to form neurites that are morphologically very similar to those induced by NGF. We found that several quantifiable features, including the average neurite length, were sensitive to varying Nrg1 and NGF concentration and were suitable surrogates of Nrg1 or NGF signaling, providing an opportunity to find specific modulators of each neurotrophic factor. As described in Kuai et al. (2010), a screen of bioactive compounds using the PC12-ErbB4-GFP neurite outgrowth phenotype, we discovered that the indolocarbazole, K252c, potentiated neuritogenesis induced by Nrg1 but had little, if any, inhibitory effect (at 10 μM) on NGF signaling. Follow-up studies found that the furanose-containing K252c analog K252a (1), a natural product originally purified from *Nocardiopsis* species (Kase et al., 1986), potentiated Nrg1-induced neuritogenesis with a much higher potency than K252c (EC$_{50}$ ~50 nM). K252a (1) was originally described as a potent protein kinase C (PKC) inhibitor (Kase et al., 1986), and like many other indolocarbazoles was later recognized as a more general kinase inhibitor with variable selectivity (Ruegg and Burgess, 1989). Subsequently, K252a (1) was found to potently inhibit Trk family members (Tapley et al., 1992), PDGF receptor (Nye et al., 1992) and HGF receptor Met (Morotti et al., 2002) signaling. Consistent with being a Trk inhibitor, K252a (1) inhibits neuronal differentiation induced by NGF and brain-derived neurotrophic factor (BDNF). Intriguingly, besides blocking NGF- and BDNF-mediated signaling, K252a (1) has also been shown to have potent neurotrophic effects in various systems (Borasio, 1990; Glicksman et al., 1993, 1995; Maroney et al., 1995; Roux et al., 2002). For example, K252a (1) has been shown to enhance neurite outgrowth in human SH-SY5Y neuroblastoma cells (Maroney et al., 1995), and in primary neuronal cultures it was found to selectively potentiate the neurotrophic effects of NT-3 (Knusel and Hefti, 1992; Pollack et al., 1999). In addition, K252a (1) has also been shown to enhance survival of dorsal root and ciliary ganglion, striatal, and forebrain primary neuron cultures (Borasio, 1990; Glicksman et al., 1993, 1995; Kaneko et al., 1997). However, despite the potential therapeutic relevance of these findings, the target(s)

responsible for these neurotrophic and neuroprotective properties of K252a (1), and the relationship of these processes to each other, has remained enigmatic. Thus, to address the target identification challenge for this important class of natural products, we sought to apply an integrative chemical genomic approach combining the use of synthetic active and inactive K252a (1)-based affinity reagents in SILAC-mediated quantitative proteomic profiling along with RNA interference (RNAi)-based loss-of-function screen to subsequently validate candidate target proteins (Ong et al., 2009; Wang et al., 2008).
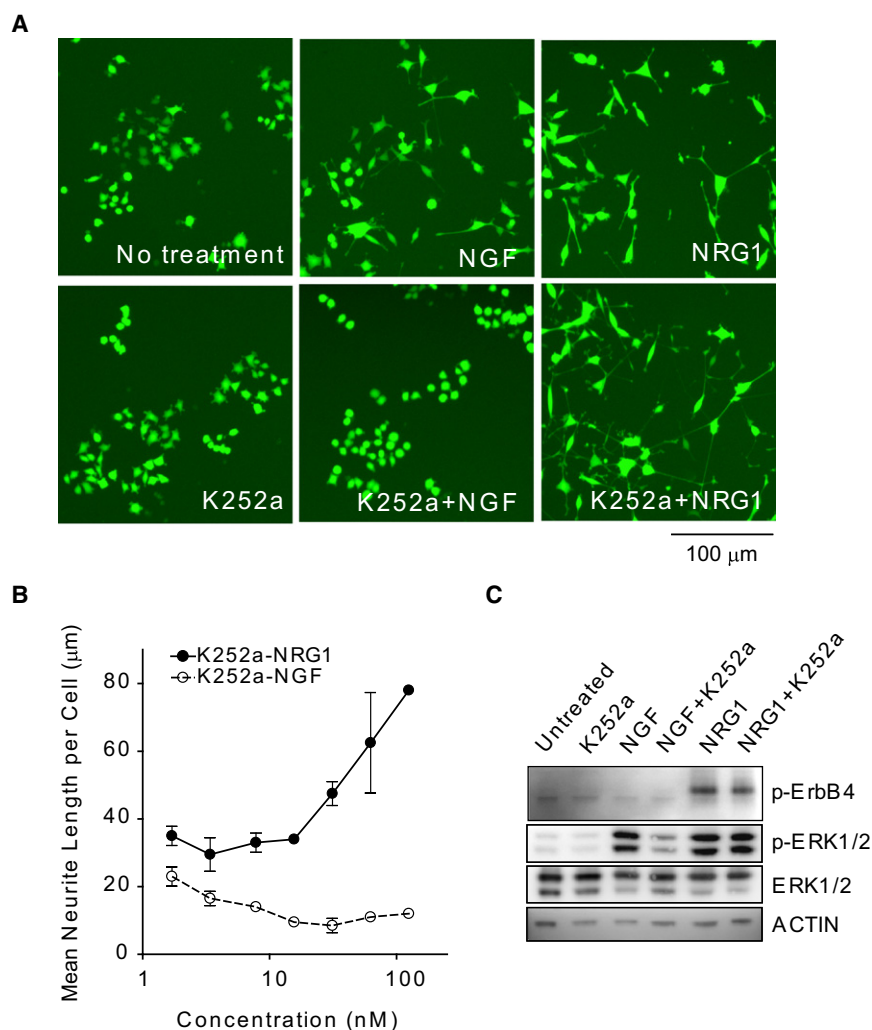
RESULTS

K252a (1) Potentiates Nrg1 but Inhibits NGF-Induced Neuritogenesis in PC12 Cells

As first described in our high throughput cell-based screening studies (Kuai et al., 2010), K252a (1) potentiates Nrg1-induced neuritogenesis in PC12 cells expressing human ErbB4 within the same dose range (1–100 nM) that inhibits NGF-induced neuritogenesis in the same cell line, whereas K252a (1) alone does not cause neurite outgrowth (Figures 1A and 1B). Consistent with previous findings (Boulton et al., 1991; Harada et al., 2001), 50 nM K252a (1) effectively inhibited NGF-induced ERK1/2 phosphorylation. However, K252a (1) did not change the autophosphorylation of ErbB4 or the downstream phosphorylation of ERK1/2 induced by Nrg1 (Figure 1C). These results suggest that the effect of K252a (1) on Nrg1-induced neurite outgrowth differs mechanistically from its previously described inhibitory effect on NGF/TrkA signaling.

The Structure-Activity Relationship (SAR) of K252a (1)

To identify cellular targets of K252a (1) mediating the potentiation of Nrg1-driven neuritogenesis, we first explored the SAR of K252a (1) in our Nrg1-ErbB4 signaling model. A small compound library containing 22 K252a (1) analogs modified at various sites was assembled to test their effectiveness in modulating Nrg1- and NGF-induced neuritogenesis (Figure 2A; see Figure S1 available online). We found that all compounds with modifications at the carbazole, indole ring, and lactam moieties were unable to potentiate neurite outgrowth induced by Nrg1 or inhibit NGF-induced neuritogenesis, consistent with a predicted binding orientation of K252a (1) to a kinase pocket (Schiering et al., 2003). Notably, compound 2 (K252a-Me), compound 7, and compound 9 modified at the C2′ position of the furanose sugar moiety also lost their activity. On the other hand, at least two of the compounds, compounds 5 (K252a-OH) and compound 8, modified at the C3′ position retained their ability to potentiated Nrg1-induced neuritogenesis.

To further explore the SAR of K252a (1), based on the finding that three analogs of K252a (1) modified at the C2′ position had diminished activities, whereas a β-hydroxy amide in the C3′ position retained its activity, we hypothesized that the C2′ position is critical for activity, whereas the C3′ position would tolerate additional functional groups. To test this hypothesis, we prepared a hybrid molecule containing both a C3′-hydroxy amide and C2′-methyl (Figure 2B, compound 23, K252a-Me-OH). As predicted, this molecule did not potentiate Nrg1-induced neurite outgrowth (Figure 2C). Interestingly, compound 2, compound 5, and compound 23 still inhibit NGF-induced neurite outgrowth

A

No treatment | NGF | NRG1
K252a | K252a+NGF | K252a+NRG1

100 μm

B

C

Untreated | K252a | NGF | NGF+K252a | NRG1 | NRG1+K252a

p-ErbB4
p-ERK1/2
ERK1/2
ACTIN

Figure 1. K252a (1) Potentiates Nrg1-Induced Neurite Outgrowth

(A) PC12-ErbB4-GFP cells were left untreated or treated with K252a (**1**) (50 nM) for 30 min, followed by 20 ng/ml of Nrg1 or NGF. Images were taken after 2 days.

(B) PC12-ErbB4-GFP cells were treated with K252a (**1**) at various concentrations as indicated for 30 min, followed by treatment with 20 ng/ml of Nrg1 (closed circles) or NGF (open circles). The mean neurite outgrowth per cell was measured after 2 day incubation. Error bars represent SEM (n = 4).

(C) PC12-ErbB4-GFP cells were left untreated or pretreated with DMSO or K252a (**1**) (50 nM) for 30 min, followed by 20 ng/ml of NGF or Nrg1, and lysed after 5 min. The levels of phospho-ErbB4 and pERK1/2 were detected by western blotting with specific antibodies. The blot was stripped and reprobed successively with ERK1/2 antibody or actin antibody.
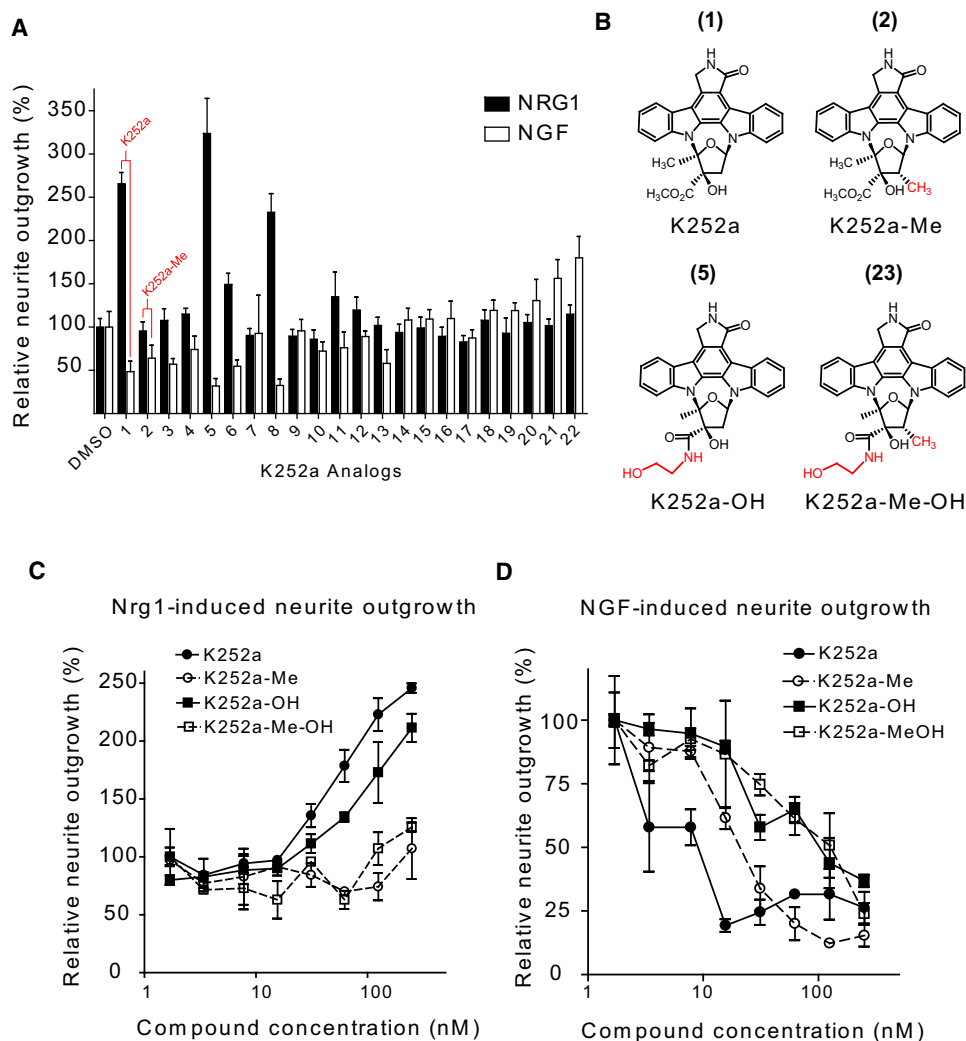
cell lysate (Figure 3B). We then compared the binding profile of the AC-K252a affinity capture probe to that of unloaded beads (bead control) using SILAC-based quantitative mass spectrometry (SILAC-target ID). A total of 114 proteins were found to bind preferentially AC-K252a beads over unloaded beads with $\log_2$ ratio >1, of which 46 of these proteins were kinases (Figure 3C). It is worth noting that the identified kinases had higher SILAC ratios than nonkinases, suggesting that immobilized K252a-OH (**5**) retained its ability to bind kinases (Kolmogorov-Smirnov test, p = 4.79 × 10^{-14}). Although this result reflects the actual binding profiles of AC-K252a versus the bead control, the large number of proteins that bound to AC-K252a did not provide immediate insight into biologically relevant binding targets to explain the effects of K252a (**1**) on Nrg1-induced neuritogenesis.

Differential SILAC-Target ID of K252a (1) and K252a-Me (2)

In order to gain insight into the targets of K252a relevant to Nrg1-induced neuritogenesis, we needed to further refine our strategy to determine biologically relevant targets. Because K252a (**1**) clearly potentiated Nrg1-driven neuritogenesis in a dose-dependent manner, but other close structural analogs did not, we speculated that only a limited number of the observed targets were relevant to this phenotype. Therefore, we designed additional experiments to further narrow down the potential targets taking advantage of the SAR we had observed for K252a (**1**) analogs and the sensitivity of SILAC-based mass spectrometry to accurately quantify differences in the binding profiles of small molecule probes (Ong et al., 2002, 2009).

Because K252a-Me (**2**) and its ethanolamide analog (**23**) lost the ability to potentiate neuritogenesis induced by Nrg1, but

at concentrations less than 100 nM, suggesting that their ability to inhibit TrkA was not diminished and highlighting the ability to uncouple different signaling pathways involved in neuritogenesis (Figure 2D). Overall, these findings reveal that not all indolocarbazole-containing compounds are able to potentiate Nrg1-mediated neuritogenesis and suggest, given the sensitivity to structural changes, that there exists a specific target mediating the biologically effects of K252a (**1**) on neuritogenesis.

K252a-Affinity Agarose Captures Multiple Kinases from Whole-Cell Lysate

Because the β-hydroxy amide (K252a-OH; **5**) retained the ability to potentiate Nrg1-induced neuritogenesis, we synthesized an affinity probe utilizing the hydroxy amide for immobilization on the solid support (see Supplemental Experimental Procedures for more details). We reasoned that this affinity bead would capture proteins from PC12-ErbB4-GFP lysate that were relevant to the Nrg1-potentiating effects of the parent compound K252a (**1**) (Figure 3A). As determined in an initial test using silver-stained SDS-PAGE, the agarose-conjugated (AC) K252a (AC-K252a) affinity probe captured multiple additional proteins compared to unloaded agarose beads subjected to the same

Figure 2. The SAR of K252a (1)
(A) PC12-ErbB4-GFP cells were treated with DMSO or a panel of 21 K252a (**1**) analogs at 100 nM for 30 min, followed by 20 ng/ml of Nrg1 (black bars) or NGF (white bars). Images were taken after 2 days and analyzed. The average neurite outgrowth of each treatment was normalized against DMSO.
(B–D) (B) Structures of K252a (**1**), K252a-Me (**2**), K252a-OH (**5**), and K252a-Me-OH (**23**). The structures of all other K252a analogs are shown in Figure S1. PC12-ErbB4-GFP cells were treated with K252a (**1**) (closed circles), K252a-Me (open circles), K252a-OH (**5**) (closed squares), or K252a-Me-OH (**23**) (open squares) at various concentrations as indicated for 30 min, followed by treatment with 20 ng/ml of Nrg1 (C) or NGF (D). The mean neurite outgrowth per cell was measured after 2 day incubation. Error bars represent SEM (n = 4).

were still able to inhibit NGF-dependent neurite outgrowth, we hypothesized that the additional methyl group of K252a-Me (**2**) alters the target selectivity compared to K252a (**1**) such that a relevant target would not bind to an K252a-Me (**2**)-based affinity capture probe. Therefore, we prepared another affinity capture probe, AC-K252a-Me, using K252a-Me-OH (**23**), to serve as an inactive analog for comparison to the AC-K252a probe using the SILAC-target ID method. Globally, the SILAC ratios of proteins quantified in both AC-K252a and AC-K252a-Me experiments were relatively consistent, suggesting that the binding profiles of these two beads were overall quite similar (Figures 3D and 3E).

The protein-binding profiles of AC-K252a and AC-K252a-Me affinity capture probes were then directly compared with three independent experiments. The first two experiments comparing

AC-K252a ("active") versus AC-K252a-Me ("inactive") were performed as technical replicates with bait swapping, an approach where a respective SILAC lysate-bead combination from one replicate was "swapped" in the second replicate. In doing so, SILAC ratios for bona fide hits are expected to flip in the two experiments, whereas false positives are not, providing a very powerful filter for quantifying false-positive interactions. Additionally, beads from the two "forward" and "reverse" experiments were washed with our standard lysis buffer (Ong et al., 2009), but in the third experiment we used a lysis buffer with 0.2% SDS for an additional higher stringency wash to strip off weaker protein binders. We also included two different bead control experimental designs using the same set of lysates: (1) "inactive" versus "active;" and (2) "active" versus bead controls, which both provided distinct information. The former directly
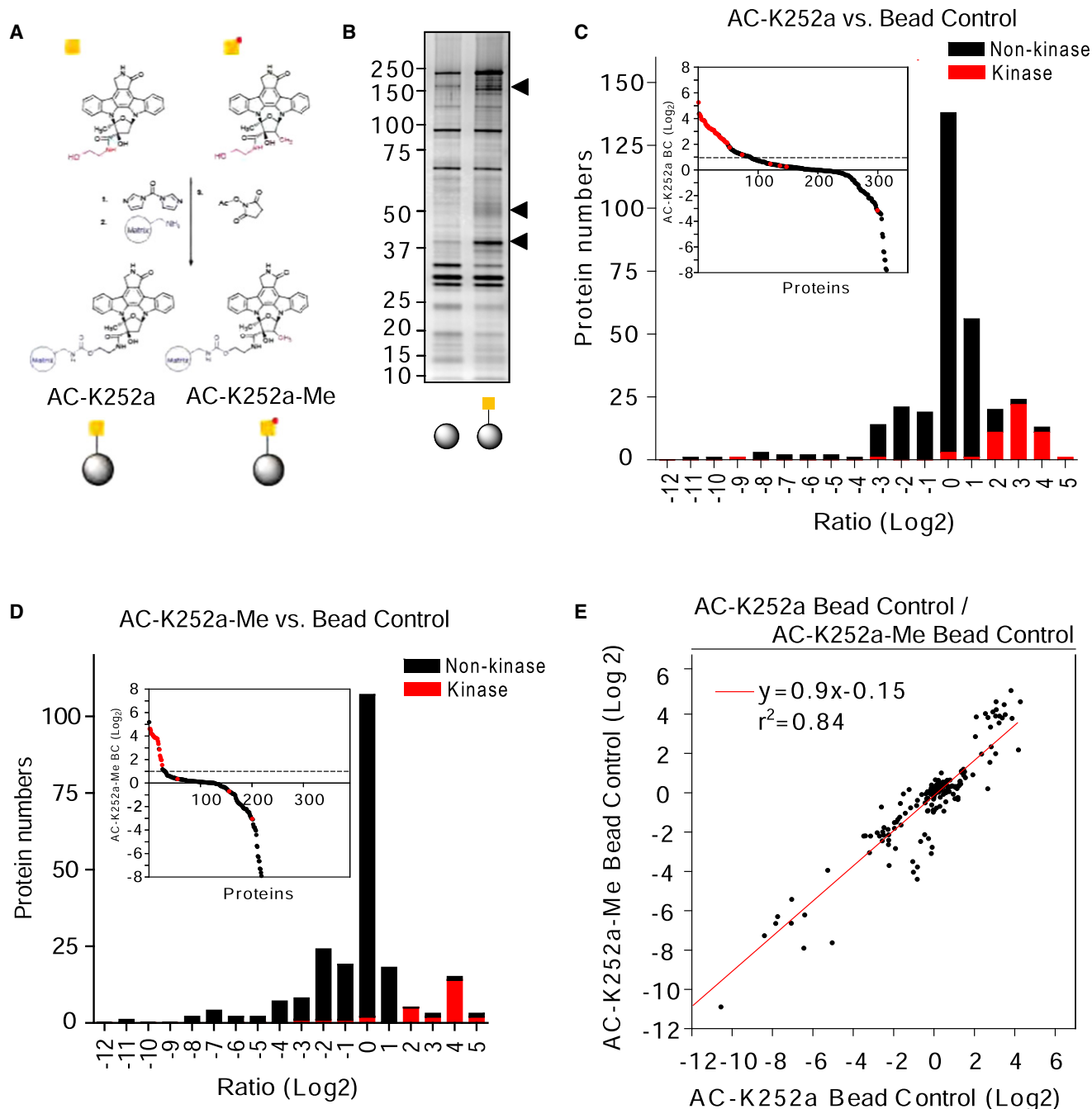
Figure 3. Kinases Captured by a K252a (1)-Based Affinity Capture Probe

(A) Scheme for generating agarose-conjugated K252a (**1**)-based (AC-K252a) and K252a-Me (**2**)-based (AC-K252a-Me) affinity capture probes.

(B) PC12-ErbB4-GFP cells were lysed and captured by unloaded agarose and AC-K252a. Eluted proteins were analyzed by SDS-PAGE with silver staining. Arrowheads represent the areas with visible differences.

(C) Stacked histogram of binding ratios of AC-K252a versus bead control (BC) detected by SILAC. Inset shows rank order of detected proteins. Kinases are represented in red. Nonkinases are represented in black.

(D) Stacked histogram of binding ratios of AC-K252a-Me versus BC detected by SILAC. Inset illustrates rank order of detected proteins. Kinases are represented in red. Nonkinases are represented in black.

(E) X axis, ratios of AC-K252a versus BC; y axis, ratio of AC-K252a-Me versus BC. Only genes that were present in both data sets were plotted and subjected to linear regression. The resulting function and correlation coefficient are included, showing globally the similarity between the two different affinity matrices.
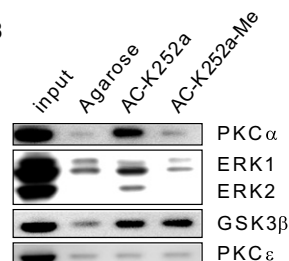
A

Protein Names	Active vs. Inactive FWD	Active vs. Inactive REV	Active vs. Inactive HS	Active Bead Control	Inactive Bead Control	Kinase
AAK1	3.4	4.0	4.4	3.9		✓
MAPK1	2.5	4.6	3.5	2.5		✓
ERK1	2.4	3.2	2.6	2.3		✓
PRKAR2A	2.4	3.8	1.2	2.3		✓
PRKAR2	2.1	3.0		2.5		✓
PRKCA	2.5	2.3		3.9		✓
PRKAC	1.7	1.2		3.8		✓
GSK3A	2.5	2.4		2.8		✓
CDK2	2.1			4.1		✓
MAP2K2	4.0			3.4		✓
MAP2K4	3.9			2.5		✓
CDC42	3.6	4.1	4.1	4.2	2.1	✓
MAP2K1	3.6	5.2	1.9	2.8	1.5	✓
AKAP8		2.2	3.4	2.2		✗
RASSF1	2.1			1.9		✗
PeS1	1.4			1.3		✗
AP2M1	1.2	1.1		1.2	-0.3	✗
AP2M1	1.4	1.2		1.0		✗

Log2 Ratio >1 ●
Log2 Ratio <0 ●

B

input Agarose AC-K252a AC-K252a-Me
PKCα
ERK1
ERK2
GSK3β
PKCε

Figure 4. Differential Affinity Enrichment with AC-K252a versus AC-K252a-Me Affinity Capture Probes

(A) Summary of identified candidate targets of K252a (**1**) based on five independent SILAC pull-down experiments. Our selection criteria (see main text) identified candidates with ratios indicating differential selectivity for active K252a (**1**) over K252a-Me (**2**) in direct comparisons with LS and HS wash conditions and from molecule versus bead control (BC) experiments. FWD, forward; REV, reverse.
(B) PC12-ErbB4-GFP cell lysate was incubated with control agarose, AC-K252a, and AC-K252a-Me agarose beads. Eluted proteins were analyzed by western blotting with specific antibodies for PKCα, ERK1/2, GSK3β, and PKCε.
See also Table S1.

members (AAK1, AP2M1, and AP2B1) of the clathrin-adaptor protein complex (Conner et al., 2003).

To begin to validate the SILAC-target ID results, we first examined the binding profiles of several identified kinases to the three beads by western blotting in whole-cell lysate pull-downs. As found in the SILAC-target ID data, PKCα, ERK1, and ERK2 were captured by AC-K252a only and substantially less by AC-K252a-Me. On the other hand, PKCε, which was not identified as enriched in either SILAC experiments, showed equal binding to all three agarose beads (Figure 4B). We also found by western blot that GSK3β (SILAC active/inactive log$_2$ ratio 0.058) was captured equally by both AC-K252a and AC-K252a-Me. Thus, these results validated the initial SILAC-target ID experiments and motivated the use of functional assays to explore the biological relevance of the interactions of proteins with K252a (**1**).

compared a protein's relative binding to the inactive and active K252a (**1**) analogs, whereas the latter enabled the determination of a protein binding to the small molecule itself relative to beads alone (i.e., bead controls). For our analyses we primarily used the SILAC ratios in bead control experiments to categorize proteins broadly as "K252a-binders" or "K252a-Me binders." Proteins identified with differential ratios in a subset of "inactive" versus "active" experiments may be false positives, and the bead control experiments can help filter these out based on the requirement that a relevant target also show significant enrichment by the affinity capture probe. Candidate targets were ultimately selected based on the following criteria: (1) log$_2$ ratio of "active" versus "inactive" greater than 1.0; (2) log$_2$ ratio of "active" versus bead control greater than 1.0; and (3) log$_2$ ratio of "active" versus bead control greater than log$_2$ ratio of "inactive" versus bead control by 1.0 (log$_2$ ratios for missing values were set at zero). With these criteria we identified 18 proteins including 13 kinases as putative targets of K252a (**1**) for Nrg1-induced neuritogenesis (Figure 4A; Table S1). Strikingly, at least three functional clusters could be detected in the short list of candidate target proteins. There were five proteins belonging to the MAPK family, three subunits (PRKAR2A, PRKAR2B, and PRKACB) of cAMP-dependent protein kinase A (PKA), and three

Functional Genomic Screen of SILAC-Target ID Candidates Using RNAi

To further clarify the relevant target of K252a (**1**), we next turned to a functional genomic screening approach using lentiviral small hairpin RNAs (shRNAs) to knock down candidate genes identified by the SILAC-target ID experiment, followed by observing the effect of loss of function using the Nrg1-induced neuritogenesis imaging assay. We reasoned that if a protein identified by the differential affinity enrichment experiment was indeed inhibited by K252a (**1**), then this approach would recapitulate the same phenotypic effect as treatment of cells with K252a (**1**) and Nrg1. With a coverage of 4–5 shRNAs tested per gene, we tested 13 of the 18 candidate targets for a total of 68 shRNAs and identified 9 hairpins covering a total of 5 separate genes (AAK1 [2 out of 4 shRNAs], AP2M1 [3 out of 5 shRNAs], PRKCA [1 out of 5 shRNAs], MAP2K2 [2 out of 5 shRNAs], and MAP2K4 [1 out of 5 shRNAs]) that substantially potentiated Nrg1-induced neurite outgrowth when silenced (Figures 5A and 5B). Because any one shRNA may have off-target effects, to control for specificity, we applied a filter requiring that more than one shRNA
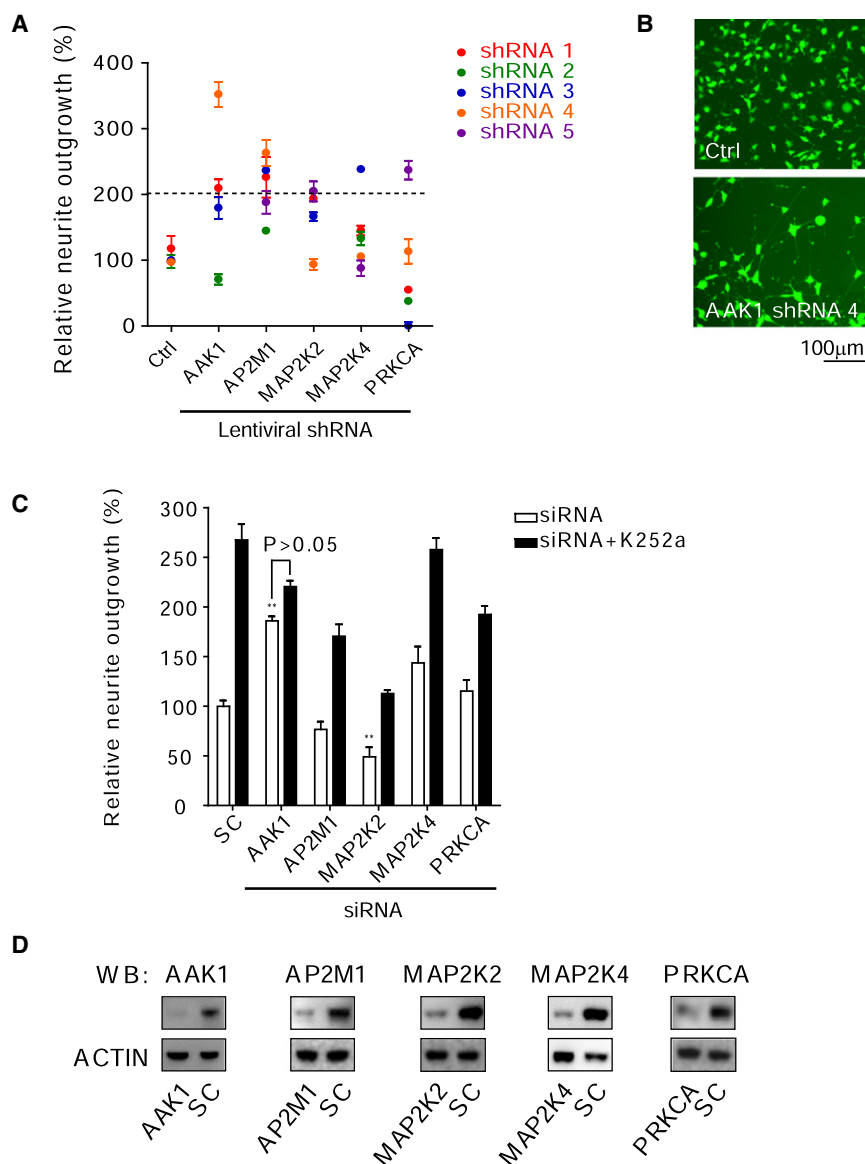
Figure 5. Knocking Down of AAK1 Potentiates Nrg1-Driven Neuritogenesis

(A) Silencing the candidate genes with lentiviral-packaged shRNAs. Five genes that have at least one corresponding shRNA hairpin that potentiates Nrg1-induced neurite outgrowth are shown (for complete results see Table S2). Cells were infected by shRNA containing viruses for 2 days, followed by treatment of 20 ng/ml Nrg1. The average neurite length in each hairpin treatment was analyzed and normalized to control a virus, which contained a nontargeting shRNA and expressed RFP (error bar represents SEM; n = 2).

(B) Representative image of PC12-ErbB4-GFP cells infected with control or AAK1 shRNA hairpin 4 and induced by Nrg1 for 2 days.

(C) PC12-ErbB4-GFP cells were transfected with siRNA targeting the five genes identified in (A) or nontargeting control siRNA (SC) (white bars), then treated with or without 100 nM K252a, followed by 20 ng/ml Nrg1 for 2 days (black bars). Average neurite length per cell of each treatment was normalized to that of the control siRNA.

(D) Western blots confirming the knockdown of each gene as indicated.

See also Figure S2.

of AAK1 potentiated Nrg1-induced neuritogenesis (Figures 5C and 5D), but silencing of the other four candidate genes, AP2M1, PRKCA, MAP2K2, and MAP2K4, did not potentiate Nrg1-induced neuritogenesis. Acknowledging the discrepancy between the two gene-silencing methods, which could be due to differences in the efficiency of knockdown or specificity of the probes, the agreement between the two methods on AAK1 strongly suggests that AAK1 is a plausible target of K252a (**1**) involved in potentiating Nrg1-induced neuritogenesis. Consistent with this notion, there was no effect of silencing AAK1 on neuritogenesis in the absence of Nrg1 treatment (data not shown), nor was there an effect of silencing AAK1 on NGF-stimulated neuritogenesis (Figure S2). These findings are consistent with the observation that K252a treatment has neither an effect on the binding of iodinated NGF nor the internalization of NGF in PC12 cells (Koizumi et al., 1988). Finally, the potentiation effect of K252a (**1**) was diminished in AAK1-silenced cells, compared to that of scrambled control and other siRNAs (Figures 5C and 5D).

Differential Inhibition of AAK1 by K252a (1) and K252a-Me (2)

Because the RNAi data suggested that AAK1 was a candidate target of K252a (**1**) involved in Nrg1-induced neuritogenesis, we further investigated whether AAK1 showed differential affinity for AC-K252a and AC-K252a-Me using direct binding experiments. We first reexamined affinity capture with these

enhanced neurite outgrowth, leaving three candidate genes. The strongest effect on neurite outgrowth in the presence of Nrg1 was obtained with multiple shRNAs targeting AAK1 (Figures 5A and 5B). Notably, three out of the five shRNAs targeting AP2M1 also met our criteria, although the magnitude of the effect was less robust. This was notable because AAK1 is a member of the ARK1/PRK1 family of serine/threonine kinases known to phosphorylate AP2M1 (adaptor-related protein complex 2, mu (μ) 1 also known as μ2), a subunit of the clathrin-adaptor complex AP2 involved in clathrin-dependent receptor endocytosis and receptor recycling (Conner and Schmid, 2002; Henderson and Conner, 2007; Ricotta et al., 2002; Smythe and Ayscough, 2003).

To confirm the results of the shRNA-mediated silencing, we subsequently retested the genes with the strongest lentiviral shRNA phenotypes using synthetic small inhibitory RNAs (siRNAs). Using this dual RNAi approach, and full validation of knockdown efficiency, we were able to confirm that silencing

probes from whole-cell lysates and found that AAK1 was specifically bound by AC-K252a and, to a much lesser extent, by AC-K252a-Me (Figure 6A). This result suggested that K252a (**1**) is associated with a complex that at least contains AAK1 but does not prove direct binding. To determine if this association was direct, we tested the affinity of both agarose beads to purified AAK1 (Δ-AID), a truncated AAK1 that included the active kinase domain with a C-terminal glutathione S-transferase (GST) tag (Conner et al., 2003). Consistent with cell lysate results, the Δ-AID AAK1-GST fusion protein was captured by AC-K252a but to a much lesser extent by AC-K252a-Me, suggesting that AAK1 indeed has a greater affinity toward K252a (**1**) than K252a-Me (**2**) (Figure 6B). Furthermore, in control experiments we found that, consistent with our SILAC experiments, purified GSK3β bound to both affinity matrices equally (Figure 6B). Finally, to test if this binding of K252a (**1**) had a functional effect on AAK1, we determined if K252a (**1**) and K252a-Me (**2**) differentially inhibited recombinant AAK1 kinase activity. Using the same recombinant Δ-AID AAK1-GST fusion protein as for the pull-down experiments, we developed an in vitro AAK1 kinase assay using a synthetic peptide substrate consisting of a sequence flanking the known AAK1 phosphorylation site (Thr156) on AP2M1. As shown in Figure 6C, K252a (**1**) potently inhibited AAK1's kinase activity with an IC_{50} <10 nM, which was three orders of magnitude more potent than the inhibition of AAK1 by K252a-Me (**2**). By contrast, both analogs inhibited recombinant GSK3β kinase activity with only a 2-fold difference in efficiency (Figure 6D), highlighting the remarkable ability of the SILAC-target ID experiment to have revealed differential binding of AAK1 to K252a (**1**) over K252a-Me (**2**), even in the context of many competing protein-small molecule interactions in a complex cell lysate.

Computational Studies of Binding of K252a (1) and K252a-Me (2) to AAK1

The integrative SILAC-target ID and functional genomic approach we employed here identified a group of kinases that can be discriminated by K252a (**1**) and K252a-Me (**2**). Although it has been established that indolocarbazoles like K252a (**1**) occupy the hydrophobic adenine-binding pocket, with the sugar moiety mimicking the hydrogen-bonding pattern of adenine in the ATP-binding site (Sanchez et al., 2006), the subtle nature and location of the 2′ methyl modification of K252a-Me (**2**) prompted us to try to gain insight into the nature of how this modification diminishes the affinity for kinase targets using computational modeling.

Using the thermodynamic integration theoretical free energy (TI) approach (Pearlman, 1998), the relative binding free energies for the unmethylated and C2′ methylated forms of K252a (**1**) were determined. The TI approach, which combines molecular dynamics with equations of elementary statistical mechanics, has been widely studied, and has been demonstrated capable of determining quantitatively reliable relative binding free energy estimates (see Supplemental Experimental Procedures for more details).

Because there is no crystallographic structure for AAK1, a homology model was created using the MOE package (2007), starting with crystal structure of the human serine-threonine kinase 16 (2BUJ) (Debreczeni et al., 2005), with which there is

25.8% total sequence homology. Initial placement of the K252a (**1**) ligand in our homology model was determined by superposition of the AAK1 homology model with the crystal structure of the tyrosine kinase domain of c-Met bound by K252a (1r0p) (Schiering et al., 2003) (Figure S3). The individual calculated free energies from this model are presented in Supplemental Experimental Procedures. From these values a net $\Delta\Delta G = \Delta G_{T2} - \Delta G_{T1} = \Delta G_{E2} - \Delta G_{E1} = 2.69 \pm 0.46$ kcal/mol was determined. In other words, adding a C2′ methyl group to K252a is 2.69 kcal/mol more unfavorable in the AAK1-bound state than in the free state, and so adding the C2′ methyl group disfavors binding by this degree. Converted to a binding constant, 2.69 kcal/mol translates to a factor of 94 or a little less than two orders of magnitude of binding affinity. From further breakdown of the thermodynamic cycle in these experiments, it appears that nearly all of the differences arise from nonbonded (nonpolar) interactions, and not from, for example, solvent rearrangement. This suggests that the difference in preference of binding to AAK1 to K252a (**1**) arises primarily from the fact that placing a methyl group at the C2′ position of K252a-Me (**2**) is sterically unfavorable and requires the adoption of a higher energy set of configuration states for either the ligand, the AAK1, or both (Figure S3). In light of the good agreement between the binding energy determined in these computational studies and the experimentally observed differences in binding affinity of one to two orders of magnitude, the sterically less favorable interactions, of K252a-Me (**2**), provide a potential explanation for the observed difference in inhibitory potency of K252a (**1**) and K252a-Me (**2**) toward AAK1 (Figure 6E).

K252a (1), but Not K252a-Me (2), Increases ErbB4 Levels in PC12-ErbB4-GFP Cells

Given the suggested role of AAK1 in clathrin-dependent receptor endocytosis (Conner and Schmid, 2002), and our demonstration for the first time of the ability of K252a (**1**) to inhibit the phosphorylation of Thr156 on AP2M1 (Figure 6C), a site known to be critically involved in regulating endocytic trafficking (Olusanya et al., 2001; Ricotta et al., 2002), we speculated that the neurotrophic effects of K252a (**1**) were related to its effect on some aspect of ErbB4 receptor trafficking. To test this hypothesis, we first examined total ErbB4 levels in PC12 cells treated with 50 nM K252a (**1**) or 50 nM K252a-Me (**2**) using western blotting. As shown in Figure 7A, treatment with K252a (**1**) dramatically increased the level of ErbB4, whereas K252a-Me (**2**) and DMSO both had no effect. Consistently, AAK1 knockdown by siRNA treatment also led to an increased level of total ErbB4 in cells (Figure 7B). This effect on ErbB4 was specific to AAK1 silencing because no effect was observed with scrambled siRNA or with a siRNA pool targeting PKCα (Figure 7B). Taken together, these results provide an additional level of similarity of the effect of K252a (**1**) treatment and AAK1 loss of function.

To gain additional insight into the basis for accumulation of ErbB4 levels, we then performed immunocytochemistry to localize ErbB4 in cells treated with K252a (**1**) or with siRNAs targeting AAK1. Interestingly, the intracytoplasmic localization of ErbB4 was greatly reduced in cells treated with K252a (**1**) and in AAK1 knockdown cells, but not in cells treated with a scrambled control siRNA or K252a-Me (**2**) (Figure 7C). These results revealed that the accumulated ErbB4 in both
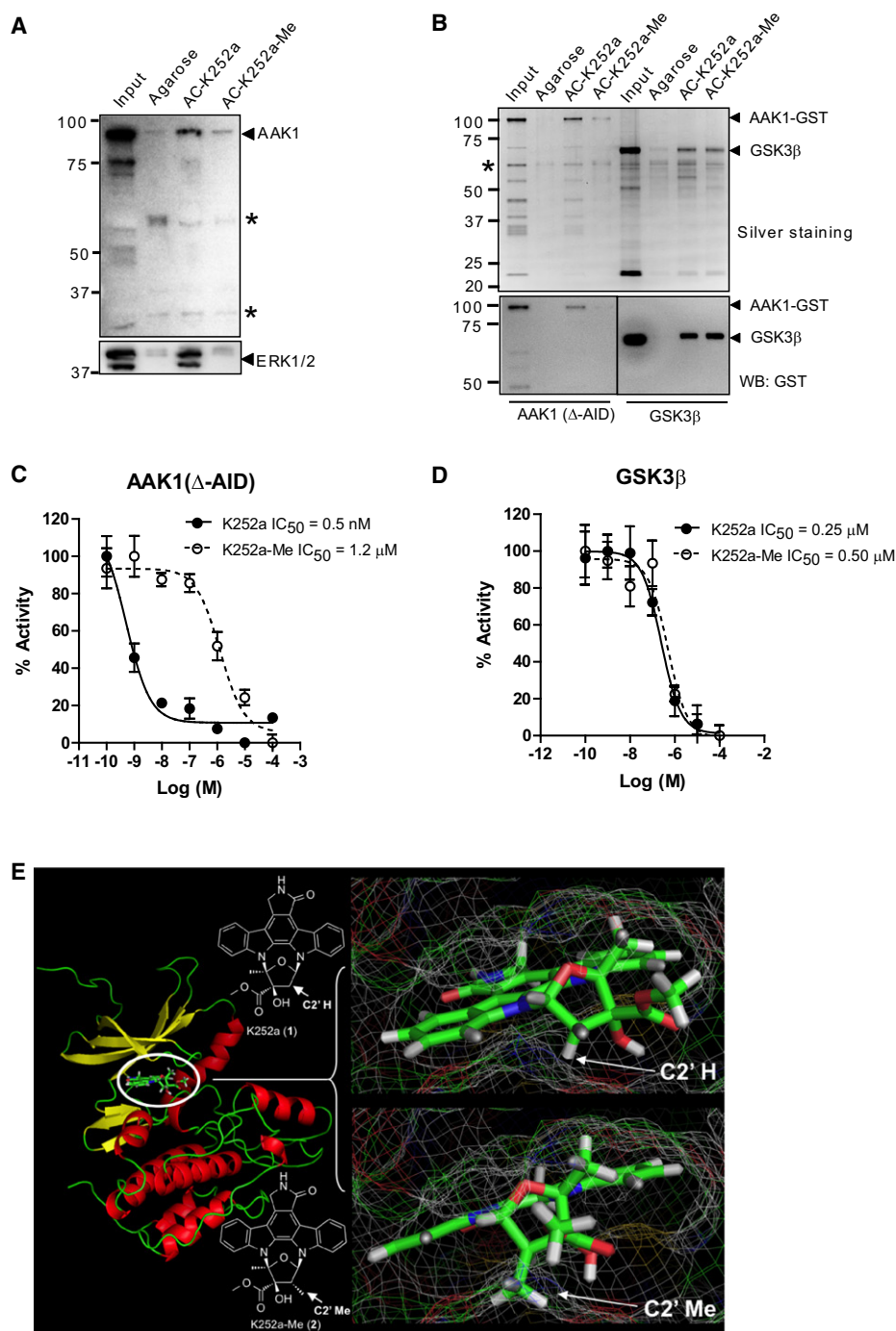
Figure 6. AAK1 Binds Directly and Specifically to K252a (1)

(A) Western blots of proteins from PC12-ErbB4-GFP cells bound by AC-K252a or AC-K252a-Me. Western blots were probed with AAK1 antisera and then stripped and reprobed with ERK1/2 antisera. AAK1 and ERK1/2 were marked with arrowheads, and nonspecific bands were marked with asterisks.

(B) GST-tagged AAK1 (Δ-AID) was affinity captured by unloaded agarose, AC-K252a, and AC-K252a-Me, and bound protein was analyzed by silver staining (upper panel) and western blotting (lower panel). A nonspecific band shown in the silver-stained gel is marked with an asterisk, and AAK1-GST was marked with an arrowhead in the western bot.

(C) Kinase activity of GST-tagged AAK1 (Δ-AID) was measured with K252a (**1**) (closed circles) or K252a-Me (**2**) (open circles) at the concentrations indicated. IC$_{50}$ for AAK1 is indicated in the legend.

(D) Kinase activity of GST-tagged GSK3β was measured with K252a (**1**) (closed circles) or K252a-Me (**2**) (open circles) at the concentrations indicated. The IC$_{50}$ for GSK3β is indicated in the legend.

(E) AAK1 homology model comparing the binding of K252a (**1**) and K252a-Me (**2**).

See also Figure S3.
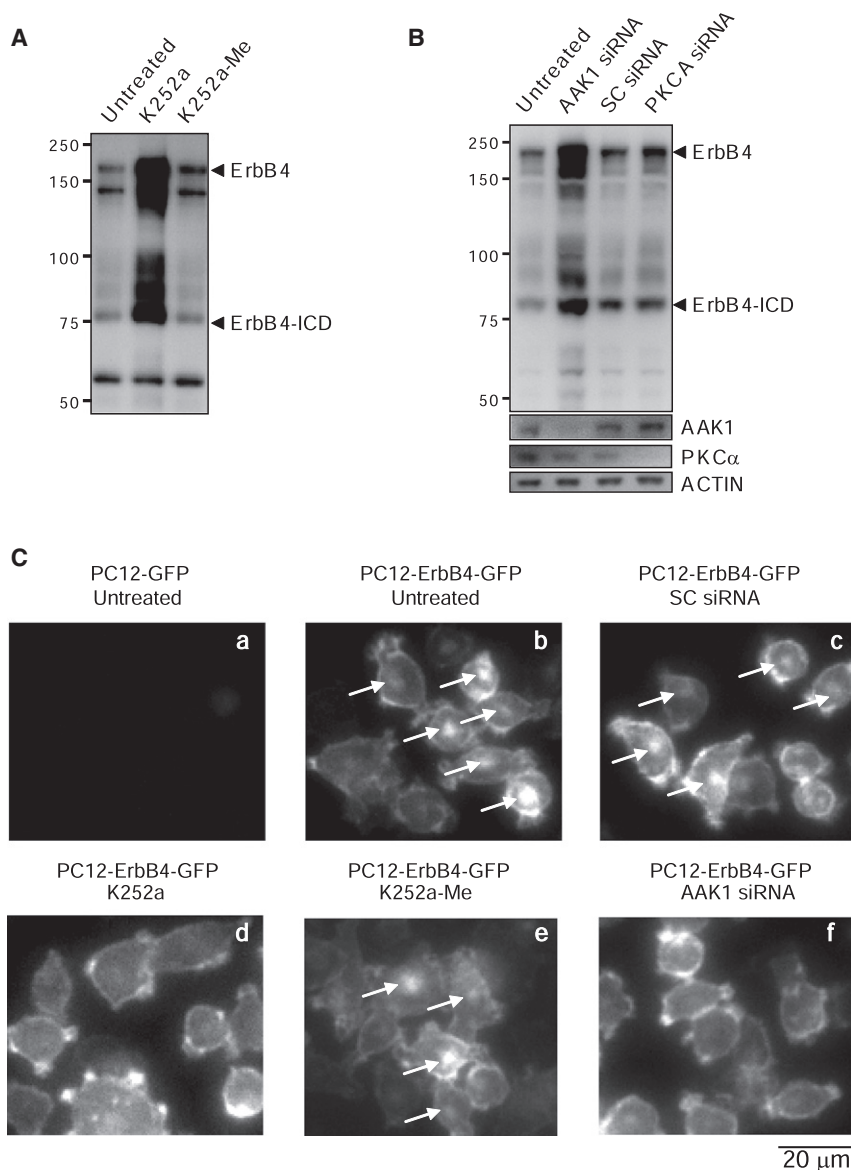
Figure 7. K252a (1) Treatment and AAK1 Knockdown Both Cause Accumulation of ErbB4 and Diminish Cytosolic Localization of ErbB4

(A) PC12-ErbB4-GFP cells were untreated or treated with 50 nM K252a (1) or 50 nM K252a-Me (2) for 12 hr, and ErbB4 was detected by western blotting with an anti-ErbB4 antibody.

(B) PC12-ErbB4-GFP cells were transfected with AAK1, PKCα, and scrambled siRNA for 2 days, and ErbB4, AAK1, PKCα, and actin were detected by western blotting.

(C) PC12-GFP control cells were left untreated (a) and PC12-ErbB4-GFP cells were untreated (b), or treated with scrambled (SC) siRNA (c), 50 nM K252a (1) (d), 50 nM K252a-Me (2) (e), or transfected with AAK1 siRNA (f). The cells were then fixed and permeabilized, followed by immunocytochemistry with an antibody that recognizes the extracellular domain of ErbB4. Images were taken at 20× magnification. Note the ErbB4 staining indicated by arrows in untreated, SC siRNA, and K252a-Me (2)-treated cells and the decreased ErbB4 levels in AAK1-siRNA-transfected and K252a (1)-treated cells. See also Figure S4.

et al., 2005) (Figure S4). This punctate labeling of PC12-ErbB4-GFP cells could be blocked by treatment with excess unlabeled Nrg1, but not EGF (data not shown). To determine if K252a (1) affected the endocytosis of Alexa 594-Nrg1, cells were pretreated for 12 hr with K252a (1), followed by a 30 min treatment at 37°C with Alexa 594-Nrg1. Following fixation and costaining for ErbB4, cells were imaged using confocal microscopy. As shown in Figure S4, K252a (1) pretreated cells showed elevated total protein and membrane levels of ErbB4 and appeared to exhibit enhanced intracellular, Alexa 594-Nrg1 punctae that colocalized with ErbB4. These results suggest that, at least to the limits of our detection methods, the stimulation of Nrg1-mediated neuritogenesis through K252a-mediated AAK1 or siRNA silencing of AAK1 does not involve blocking Nrg1-induced ErbB4 endocytosis.

K252a (1)-treated and AAK1 knockdown cells was mainly located in close proximity or within the outer plasma membrane. Again, the correspondence between the K252a (1) and siRNA cellular ErbB4 localization phenotypes further supports the conclusion of the relevance of AAK1 as a target involved in potentiation of Nrg1-induced neuritogenesis.

Finally, to further investigate the possible mechanism through which K252a-mediated inhibition of AAK1 potentiates Nrg1-induced signaling and neuritogenesis, we sought to determine if K252a (1) treatment was capable of altering ErbB4 endocytosis. Previously, fluorescently labeled Nrg1 has been shown to be coendocytosed with ErbB4 in HEK293 cells and in rat hippocampal neurons (Liu et al., 2007; Yang et al., 2005). Consistent with these findings, after incubation with Alexa 594-Nrg1 at 37°C for 30 min, PC12-ErbB4-GFP cells, but not PC12-GFP cells that lack the ErbB4 receptor, exhibited numerous fluorescent punctae typical for endocytic particles (Liu et al., 2007; Yang

DISCUSSION

In the present study we characterized the ability of K252a (1), an extensively used indolocarbazole natural product, to potentiate Nrg1-induced neuritogenesis. Neuritogenesis, the earliest stage of neural cell differentiation, involves the formation of neurites that play an important role in neural migration and patterning. Despite the importance of neuritogenesis for proper neural circuit formation, our understanding of the underlying molecular mechanisms and our ability to modulate them remain limited. Gaining an understanding of the molecular machinery and mechanisms that generate and remodel neural circuits is necessary

for the development of small molecule probes that can modulate these processes for potential therapeutic benefit.

By exploring the chemical space around K252a (**1**) (Figure 2A; Figure S1), we found that the C3′ position of the furanose moiety could accommodate certain modifications while maintaining cellular activity. In particular the β-hydroxy amide analog (**5**) allowed us to immobilize K252a (**1**) to generate an affinity capture probe (AC-K252a) to try to enrich for protein binders. Use of the AC-K252a probe was found to enrich for at least 46 kinases from cellular lysates, as detected by SILAC-based quantitative mass spectrometry, consistent with the expectation that indolocarbazoles such as K252a (**1**) interact with many kinases. Because the C2′ position of the furanose moiety of K252a (**1**) was sensitive to modification with even the addition of methyl group at this site being capable of causing a loss of activity with respect to Nrg1-induced neuritogenesis, this prompted us to use an AC-K252a-Me affinity capture probe to eliminate irrelevant targets based on the hypothesis that K252a-Me (**2**) did not inhibit the relevant targets. With quantitative mass spectrometry enabled through the use of SILAC, we further narrowed down our candidate list to 18 proteins, including 13 kinases, which preferentially bind to K252a (**1**) over K252a-Me (**2**). This demonstrates the effectiveness of using a structurally similar, but biologically inactive, analog of the small molecule of interest to dissect out irrelevant targets when using the SILAC-target ID methodology. In addition the surface difference between immobilized active compound and inactive compound is presumably more similar than that of unloaded agarose beads, therefore reducing false-positive identification. Based on these reasons, the combination of SILAC-based quantitative mass spectrometry with affinity enrichment with active and inactive compounds provides a useful target identification strategy. Alternatively, competition with soluble competitor is another strategy that has proven successful for target identification using the SILAC approach (Ong et al., 2009), particularly if the quantity and solubility of competitor are not a concern and an inactive structural analog is not known.

During the target validation process, we used a lentiviral-mediated RNAi loss-of-function screen to validate candidate target proteins and found that AAK1 reproducibly potentiated Nrg1-driven neuritogenesis when knocked down with both lentiviral shRNAs and siRNAs. Our follow-up characterization confirmed the SILAC affinity purification studies through the demonstration of a direct and functional interaction of AAK1 with K252a (**1**) (Figure 6A). Furthermore, the relevance of AAK1 as a target of K252a (**1**) is also supported by our computational modeling of the interaction of K252a (**1**) and K252a-Me (**2**) with a homology model of AAK1, which revealed subtle but notable differences in the binding energy and mode between the two small molecules and the ATP-binding site of AAK1.

The sensitivity and specificity of the SILAC-target ID assay are afforded by the use of mild buffer conditions that may allow the observation of weaker small molecule-protein interactions and multiprotein complexes, whereas quantitative mass spectrometry-based abundance measurements determine the specificity of proteins bound to affinity baits (Ong et al., 2009). In agreement with these attributes, and providing further support that AAK1 is a cellular target of K252a (**1**) involved in mediating its neurotrophic effect, the SILAC-target ID experiments also yielded

AP2M1 and AP2B1, two known binding partners of AAK1, as binders to the Ac-K252a (**1**) but not the AC-K252a-Me (**2**) affinity capture probes.

AAK1 belongs to the ARK/PRK family of serine/threonine kinases that share homologies in their kinase domain but exhibit a diverse range of other functional domains. In yeast, ARK and PRK have been shown to function in endocytosis by regulating actin dynamics. However, in mammalian cells, to our knowledge, there is currently no evidence to suggest that AAK1 influences actin dynamics. AAK1 kinase activity is robustly stimulated by clathrin, suggesting a key role for AAK1 in regulating clathrin-mediated endocytosis (Conner et al., 2003), although it remains unclear if the kinase activity of AAK1 is required for the uptake of any particular receptor, which is an active area of investigation. Given our isolation of AAK1 and AP2 adaptor complex-associated proteins with our K252a-based affinity probes, and the observation of the elevated total levels of ErbB4 and its redistribution toward cellular membranes upon treatment with K252a (**1**) and RNAi-mediated gene silencing of AAK1, it is tempting to speculate that the loss of function of AAK1 leads to an ErbB4 internalization defect due to altered clathrin-mediated endocytosis (Conner and Schmid, 2002; Ricotta et al., 2002; Smythe and Ayscough, 2003). Although the mechanism of internalization of ErbB4 is poorly understood (Baulida et al., 1996; Sorkin and Goh, 2008), several recent studies have demonstrated that endocytosis of ErbB4 does occur in various cellular systems, and regulation of this process may be a critical component of the dynamic regulation of Nrg1-ErbB4 signaling, particularly in neurons (Liu et al., 2007; Longart et al., 2007; Sundvall et al., 2008).

However, besides playing a key role in regulating AP2 recruitment to endocytic cargo through phosphorylation of μ2 (Ricotta et al., 2002), AAK1 has been shown to function at multiple steps in receptor transport including receptor recycling from the early endosome and pathways involved in protein degradation (Henderson and Conner, 2007). In support of the interpretation that the effect of K252a-mediated AAK1 inhibition does not block Nrg1-stimulated ErbB4 endocytosis, previous studies have shown that the inhibition of ErbB4 endocytosis attenuated Nrg1-induced activation of ERK1/2 (Liu et al., 2007), whereas we did not observe such attenuation with K252a (**1**) treatment (Figure 1). Thus, our data suggest that the observed accumulation of ErbB4 on the surface of the cells and the observed increase in total ErbB4 protein levels are ultimately more likely the result of blocking a critical step in ErbB4 trafficking. One possibility for this block is that K252a-mediated AAK1 inhibition causes alteration in endosomal sorting of the ErbB4 receptor, possibly thereby directing ErbB4 back to the plasma membrane. Alternatively, AAK1 inhibition may result in a failure to direct transport of ErbB4 toward degradation in the lysosome. At present, without more detailed pulse-chase labeling studies, higher-resolution imaging, and investigation of the kinetics of ErbB4 trafficking, we cannot distinguish between these possibilities and cannot rigorously rule out a role for K252a-mediated inhibition of AAK1 in blocking ErbB4 endocytosis. Such studies would also benefit from the identification of selective AAK1 probes, which remains an area for future studies.

Similar to other members of the EGFR(/ErbB) family of receptor tyrosine kinases, signal transduction of the ErbB4

receptor upon binding of its cognate ligand Nrg1 results in phosphorylation of cytoplasmic tyrosine residues to afford coupling to downstream singling molecules. Therefore, if ErbB4's kinase activity was modulated by AAK1 inhibition, this would be expected to result in a change in the phosphorylation state of ErbB4. However, we see no evidence for an increase in the tyrosine phosphorylation levels of ErbB4 upon treatment with K252a alone (Figure 1C), suggesting that AAK1 inhibition does not itself directly affect ErbB4 kinase activity. Furthermore, if ErbB4's kinase activity is modulated by AAK1, K252a treatment alone should have downstream functional consequences of ErbB4 signaling, including ERK1/2 phosphorylation and neuritogenesis. As shown, neither the treatment of cells with K252a alone (Figure 1) nor silencing of AAK1 with siRNAs (Figure 5) had an effect on neuritogenesis or downstream ERK1/2 activation in the absence of Nrg1 treatment, suggesting again that AAK1 inhibition does itself not affect ErbB4 kinase activity.

Indolocarbazoles, such as K252a (**1**), belong to a family of natural products that have been extensively studied in the past decade, owing in part due to their wide-ranging biological activities. With their planar structure and indole rings, they have been shown through crystallographic studies to bind in the ATP-binding pocket in a competitive manner with ATP. Given the similarity of ATP-binding pockets among kinases, many indolocarbazole inhibitors possess high potency but low selectivity among the members of the kinome. For example, staurosporine, the first indolocarbazole isolated in 1977, was shown to have affinity with most of the kinases in human kinome (Fabian et al., 2005; Karaman et al., 2008). After first being demonstrated to be an inhibitor in the nanomolar range of NGF-induced biochemical effects and neurite outgrowth in PC12 cells (Cho et al., 1989; Hashimoto, 1988; Koizumi et al., 1988; Lazarovici et al., 1989; Miyasaka et al., 1990; Smith et al., 1989), Berg et al. (1992) went on to demonstrate that K252a directly inhibits NGF-induced Trk receptor tyrosine phosphorylation in cells and kinase activity in vitro in a dose-dependent manner. These early studies also suggested that K252a may have one or more additional cellular targets involved in the process of signal transduction (Berg et al., 1992). It was also recognized that improved selectivity can be obtained by modifying the mode of ligand interaction. A wide variety of structures within the indolocarbazole family have been found to have selectivity for particular kinases, such as PKC isozymes (Zhang et al., 2005), CDKs (Al-awar et al., 2004), GSK3β (Kuo et al., 2003), VEGF-R2 tyrosine kinase (Gingrich et al., 2003), and mixed lineage kinases (MLKs) (Murakata et al., 2002). A number of indolocarbazoles have been or are still in clinical development for disease indications in the area of oncology and neurodegeneration. In the context of developing agents to treat neurodegenerative disorders, previous studies have evaluated the neuroprotective effects of a series of 3,9-disubstitued K252a (**1**) derivatives, as measured by the in vitro enhancement of choline acetyltransferase activity in primary rat spinal cord and forebrain cultures (Kaneko et al., 1997). These compounds, while showing increased neurotrophic activity over K252a (**1**), showed decreased ability to inhibit Trk kinase activity. One of these K252a (**1**) derivatives known as CEP1347 (compound **10**) has been reported to have neuroprotective effects through inhibiting MLK family members (Roux et al., 2002). However, CEP1347 (compound

10) did not potentiate Nrg1-induced neurite outgrowth in our PC12-ErbB4-GFP cellular assays. This result suggests that the potentiation by K252a (**1**) of Nrg1-induced neuritogenesis is distinct from the neuroprotective features reported previously for 3,9-disubstitued K252a (**1**) derivatives. This conclusion is further supported by the fact that we found no support for MLKs as being relevant targets of K252a (**1**) in PC12 cells from our SILAC-based target identification studies.

In now classic experiments in the field of signal transduction (Greene and Tischler, 1976; Heasley and Johnson, 1992; Kaplan et al., 1991a, 1991b; Traverse et al., 1992), sustained activation of ERK1/2 was shown to occur in response to NGF, whereas EGF treatment, which induces a mitogenic response leading to cell proliferation, led to a short-lived ERK1/2 activation. These observations provided a model system for the dissection of how activation of certain receptors that couple to the same effector signaling molecules can lead to differential biological outcomes.

In our study the same small molecule probe, K252a (**1**), leads to differential biological outcomes in a manner dependent upon the nature of the signal transduction cascade activated by different neurotrophic factors. With NGF treatment, because K252a (**1**) has a direct inhibitory effect on the tyrosine kinase activity of the Trk receptor that blocks the sustained activation of ERK1/2 that normally occurs upon NGF treatment (Berg et al., 1992), the observed dose-dependent inhibition of neuritogenesis and correlation we observe in Figure 1B between loss of ERK1/2 phosphorylation and lack of increased neurite length are expected. In contrast, with Nrg1 treatment, which as shown in Figure 1C, also causes activation of ERK1/2, K252a (**1**) treatment does not inhibit ERK1/2 activation but instead maintains the level of ERK1/2 activation, leading to an increase in neurite length (Figure 1B). These results demonstrating distinct effects of K252a (**1**) on different signaling pathways are consistent with the earlier observation that EGF and bFGF-stimulated protein tyrosine phosphorylation in PC12 cells was unaffected by K252a (**1**) treatment (Berg et al., 1992).

In the case of Nrg1/ErbB4 signaling, because both K252a (**1**) treatment and AAK1 siRNA-mediated gene silencing led to increased levels of ErbB4 (Figures 7A and 7B) that can be observed on the cell membrane (Figure 7C), it is plausible that K252a (**1**)-mediated inhibition of AAK1 leads to a sustained activation by ErbB4 of downstream signaling, including the activation of ERK1/2, leading to enhanced Nrg1-mediated neuritogenesis. This model for the biological effects of K252a (**1**) on Nrg1-dependent neurotrophic factor signaling highlights the fact that, despite different neurotrophic factors having shared signal transduction pathways downstream from their receptors, it is possible to identify small molecule probes that can target a unique aspect of the underling molecular mechanisms. Identification of these targets, such as AAK1 for Nrg1/ErbB4 signaling, may lead to novel types of therapeutic agents for a variety of CNS disorders in which there is dysfunction of neurotrophic factor signaling.

SIGNIFICANCE

The discovery of low-molecular weight small molecules with neurotrophic modulating activity represents a valuable

opportunity for testing the relevance of neurotrophic factor-signaling mechanisms to human disease. The blood-brain barrier impermeability and overall pharmacokinetic characteristics of most polypeptide-based neurotrophic factors limit their ability to be administered systemically for the treatment of many CNS disorders. In the case of schizophrenia (OMIM 181500), a highly heritable and devastating neuropsychiatric disorder, although there is still conflicting genetic evidence, several genetic, transgenic mouse, and postmortem human brain studies have suggested Nrg1 and ErbB4 as putative susceptibility genes (Mei and Xiong, 2008; Buonanno, 2010). Given the observations that Nrg1 regulates excitatory pyramidal neurons in the prefrontal cortex via presynaptic ErbB4 receptors on parvalbumin-positive GABAergic interneurons (Woo et al., 2007), as well as recent findings that have shown the ablation of ErbB4 in parvalbumin-positive interneurons in mice results in animals that exhibit schizophrenia-relevant phenotypes (e.g., hyperactivity, impaired working memory, and deficit in prepulse inhibition) (Wen et al., 2010), the use of K252a (1) and inhibition of AAK1-mediated signaling may provide further insight into the role of Nrg1 and ErbB4 in the pathogenesis of psychotic illnesses. In addition a recent genome-wide association study of factors influencing the age of onset of Parkinson's disease (OMIM 168600) identified single nucleotide polymorphisms in an intron of the AAK1 gene, highlighting a potentially important role for regulation of neurotrophic factor signaling in other CNS disorders (Latourelle et al., 2009). Thus, the integrative chemical genomic and proteomic approach described here has the potential to be broadly applicable to the identification of functionally important targets and mechanisms for disease intervention.

EXPERIMENTAL PROCEDURES

Materials
PC12 cells (subclone Neuroscreen-1) were obtained from Cellomics (now Thermo Fisher Scientific, Pittsburgh, PA). PC12-ErbB4-GFP and PC12-GFP stable cell lines were generated previously (Kuai et al., 2010). Antibodies used were: rabbit anti-ErbB4 c-18, rabbit anti-phospho-ErbB4 (Santa Cruz Biotechnology, Santa Cruz, CA; #SC283, #SC33040); rabbit anti-phospho-p42/44 MAPK, rabbit anti-p42 MAPK, rabbit anti-PKCα, rabbit anti-PKCε, rabbit anti-GSK3β (Cell Signaling Technology; #9106, #4695, #2056, #2683, and #9315, respectively); and mouse anti-actin (Sigma; A1798). AAK1 rabbit anti-sera and the Δ-AID AAK1-GST construct were obtained from Dr. Sean D. Conner (University of Minnesota, Minneapolis, MN,). The EGF domain of Nrg1β1 (corresponding to amino acid residues 176–246 of neuregulin-1β1) was expressed and purified from *E. coli* (R&D Systems; #396-HB-CF) and reconstituted in phosphate-buffered saline (PBS) with 0.1% bovine serum albumin as a nonspecific carrier and frozen in aliquots at −20°C. Murine 2.5S Nerve growth factor (Promega; G5141) was reconstituted in PBS 0.1% bovine serum albumin as a nonspecific carrier and frozen in aliquots at −20°C. siRNA SmartPools for specified target genes (AAK1: L-105612-01; AP2M1: L-096180-01; PKCα: L-080129-00; MAP2K4: L-084558-00; MAP2K2: L-088324-01), nontargeting (D-001810-10), and DharmaFECT2 (T-2002-03) were purchased from Dharmacon (Chicago, IL). Lentiviral shRNAs used are summarized in Table S2. Hairpin sequences can be retrieved from http://broadinstitute.org/genome_bio/trc/publicSearchForHairpinsForm.php.

Cell Culturing and Stable Cell Line Generation
PC12 cells were maintained in RPMI 1640 media (GIBCO; 22400) containing 10% heat-inactivated horse serum (GIBCO; 26050), 5% heat-inactivated fetal bovine serum (GIBCO; 16140), and 1% penicillin/streptomycin (GIBCO;

10378) referred to here as RPMI+. For PC12-ErbB4-GFP and PC12-GFP, 1% penicillin/streptomycin was replaced with 750 μg/ml gentamicin (GIBCO; 15750). Cells were passaged at 80%–90% confluency and incubated at 37°C in 5% CO_2. Media were changed every 3 days. PC12 cells were cotransfected with pcDNA3-ErbB4-neomycin or pcDNA3-neomycin and pcDNA-GFP using FuGene 6 transfection reagent (Roche Diagnostics; 11814443). Cells that express the neomycin-resistant gene were selected and maintained in same culture media with substitution of 750 μg/ml gentamicin. After 2 weeks of gentamicin selection, cells were further selected by fluorescence-activated cell sorting (FACS) using a MoFlo Cell Sorter (Dako, Denmark) of the top 5% most strongly GFP-expressing cells. The expression of GFP in the resulting cell population, PC12-ErbB4-GFP, and PC12-GFP was observed to be stable for at least 50 passages.

Western Blotting and Silver Staining
Cells were lysed with RIPA buffer (Pierce Technology, Rockford, IL; 89901) containing one tablet per 10 ml protease inhibitor cocktail Complete Mini (Roche Applied Science; 11836153). For phosphoprotein analysis, Halt Phosphatase Inhibitor Cocktail (Pierce Technology; 78415) was also included. Cell lysates were cleared by centrifugation at 15,000 rpm for 30 min at 4°C, followed by addition of LDS sample buffer (Invitrogen; NP008) for direct analysis. Samples were separated using a 4%–12% gradient gel (Invitrogen) and SDS-PAGE and transferred to a polyvinylidene difluoride (PVDF; Schleicher & Schnell; 10413096) membrane in 25 mM Tris, 192 mM glycine, and 20% methanol. The membrane was probed with specific primary antibodies according to specified recipes provided by their venders and then horseradish peroxidase-conjugated secondary antibody to mouse or rabbit IgG (GE Healthcare, Piscataway, NJ; NA934V and NA931V). Target protein bands were detected with SuperSignal West Femto Max Sensitivity Substrate (Pierce Technology; 34095). Silver staining was performed according to manufacturer protocol (Invitrogen; SilverQuest Silver Staining Kit, LC6070).

Lentiviral shRNA Knockdown of Target Genes
Lentiviral shRNA experiments were performed as previously described (Moffat et al., 2006) with modifications compatible with the use of automatic neurite detection algorithms. Cells were typically seeded at a density of 4000 cells/cm^2 and incubated for 12 hr. Lentiviruses were added at a multiplicity of infection (MOI) ~1, and the plate was centrifuged at 2000 rpm for 20 min before continued incubation in 37°C. The cells were incubated for 24 hr at 37°C in 5% CO_2 and treated with neurotrophic factors together with 2 μg/ml puromycin for neuritogenesis measurement after 48 hr, or directly lysed for western blot analysis.

siRNA Knockdown of Target Genes
Cells were typically seeded at a density of 4000 cells/cm^2 and incubated for 12 hr. siRNAs were prepared as a 1 μM solution in serum-free medium, and DharmaFECT2 was diluted 1:50 (v/v) with serum-free medium. Both solutions were incubated at room temperature for 5 min before mixing thoroughly and incubated for an additional 20 min. The transfection mix was then added to cell cultures at 1:5 (v/v). The cells were incubated for 24 hr at 37°C in 5% CO_2 and treated with neurotrophic factors or directly lysed for western blot analysis.

Cell Imaging and Neurite Measurements
Cells were seeded in black, clear bottom, tissue culture-treated 96-well (Corning; 3904) or 384-well (Corning; 3712) plates at typical density of 4000 cell/cm^2 corresponding to approximately 1200 cells per well of a 96-well plate in 100 μl of media and 300 cells per well of a 384-well plate in 40 μl of RPMI medium. Even distribution of cells was achieved by a quick centrifuge at 500 rpm using a tabletop centrifuge (Sorvall, LegendRT) and multiwell plate adaptors shortly after cell seeding. Cells were then incubated for 12 hr followed by treatment with growth factors or compounds as indicated. At specified time points, fluorescent images were taken using an ImageXpress 5000A or ImageXpress Micro automated microscopy (Molecular Devices) either manually or laser-based autofocus with a Nikon 4× objective (ELWD S Fluor/0.20 NA) and an image acquisition time of 150 ms or as specified. Transmitted light images were taken using an ImageXpress Micro (Molecular Devices) with an attached transmitted light device with a Nikon 4× objective (ELWD S Fluor/0.20 NA).

Neurite detection and analysis were performed with MetaXpress (Molecular Devices) using the "Neurite Detection" analysis module. Cell bodies were specified as pixel blocks of maximum width 40 μm, minimum area 200 μm², and pixel intensities 1000 U above local background. Neurites were specified as linear objects with maximum width 3 μm and pixel intensities 500 U above the local background of the object being measured.

SILAC Media Preparation and Cell Culture Conditions

We followed all standard SILAC media preparation and labeling steps as previously described (Ong and Mann, 2006), except that 750 μg/ml gentamicin was supplemented for maintenance of the transfected ErbB4 plasmid. ErbB4-PC12 cells were grown in RPMI-labeling media, prepared as described above, supplemented with 2 mM L-glutamine, and 10% dialyzed fetal bovine serum plus antibiotics, in a humidified atmosphere with 5% CO_2 in air. Cells were grown for at least six cell divisions in labeling media.

Preparation of Affinity Matrices

See Supplemental Experimental Procedures.

Biochemical Enrichment with Small Molecule Affinity Capture Probes

Separate cultures of ErbB4-PC12 cells SILAC labeled either with L-arginine and L-lysine (light) or L-arginine-$^{13}C_6$ and L-lysine-$^{13}C_6$-$^{15}N_2$ (heavy) were lysed in ice-chilled ModRIPA buffer (low-stringency [LS] buffer) containing 1% NP-40, 0.1% sodium deoxycholate, 150 mM NaCl, 1 mM EDTA, 50 mM Tris (pH 7.5), and protease inhibitors (CompleteTM tablets; Roche Applied Science, Indianapolis, IN). Lysates were vortexed intermittently while chilled on ice for 10 min and clarified by spinning at 14,000 × g. Protein concentrations of light and heavy lysates were estimated with the Protein Assay Dye Reagent Concentrate (Bio-Rad, Hercules, CA) and equalized.

For bead control SILAC-Target ID affinity pull-down experiments, 2 mg of light ErbB4-PC12 lysate was incubated with 25 μl of 50% slurry of empty bead, whereas 2 mg of heavy lysate was incubated with 25 μl of 50% of either AC-K252a ("active") or AC-K252a-Me ("inactive") small molecule affinity capture probes. In "inactive" K252a-Me versus "active" AC-K252a experiments, two LS wash experiments were performed where the ModRIPA lysis buffer was used to wash the pull-downs. These two sets of pull-downs were performed in "forward" and "reverse" modes, with bait swapping using the same sets of lysates and beads but swapping the respective combinations of lysates-beads in the two replicate experiments. Affinity enrichments were incubated overnight (~16 hr) on an end-over-end rotator at 4°C. Following incubation the tubes were spun at 1000 × g on a benchtop centrifuge to pellet the beads. The supernatant was aspirated carefully. Beads were combined at the first wash for subsequent washing steps. In the third experiment a wash buffer (high stringency [HS]) containing ModRIPA and 0.2% SDS was used to wash beads instead. After the third and final wash, beads were collected by spinning at 1000 × g, and the wash was aspirated, leaving approximately 20 μl of buffer in the tube.

One-Dimensional SDS-PAGE and Mass Spectrometric Analysis

Proteins were reduced and alkylated, on beads, in 2 mM DTT and 10 mM iodoacetamide, respectively. One-part LDS buffer (Invitrogen) was added to three-parts sample (including beads), and tubes were heated to 70°C for 10 min. Proteins were resolved on a 4%–12% gradient, 1.5 mm thick Bis-Tris gel with MES running buffer (NuPAGE; Invitrogen) and Coomassie stained (Simply Blue; Invitrogen). Gel lanes were excised into six pieces and then further cut into 1.5 mm cubes. The gel pieces were further destained in a solution containing 50% EtOH and 50% 50 mM ammonium bicarbonate, then dehydrated in 100% EtOH before addition of sufficient trypsin (12.5 ng/μl) to swell the gel pieces completely. An additional 100 μl of 50 mM ammonium bicarbonate was added before incubating at 37°C overnight on a thermomixer (Eppendorf). Enzymatic digestion was stopped by the addition of 100 μl of 1% TFA to tubes. A second extraction with 300 μl of 0.1% TFA was combined with the first extract, and the peptides from each gel slice were cleaned up on C18 StageTips (Rappsilber et al., 2007). Peptides were eluted in 50 μl of 80% acetonitrile/0.1% TFA and dried down in an evaporative centrifuge to remove organic solvents. The peptides were then resuspended by vortexing in 7 μl of 0.1% TFA and analyzed by nanoflow-LCMS with an Agilent 1100 with auto-

sampler and a LTQ-Orbitrap. Peptides were resolved on a 10 cm column, made in-house by packing a self-pulled 75 μm I.D. capillary, 15 μm tip (P-2000 laser-based puller; Sutter Instruments) column with 3 μm Reprosil-C18-AQ beads (Dr. Maisch GmbH, Ammerbuch-Entringen, Germany) with an analytical flow rate of 200 nl/min and a 58 min linear gradient (~0.57% B/min) from 0.1% formic acid in water to 0.1% formic acid/90% acetonitrile. The run time was 108 min for a single sample, including sample loading and column reconditioning.

We used a mass spectrometry method with a master Orbitrap full scan (60,000 resolution) and data-dependent LTQ MS/MS scans for the top five precursors (excluding z = 1) from the Orbitrap scan. Each cycle was approximately 2 s long. We used MaxQuant (Cox and Mann, 2008) (v.1.0.12.31) with Mascot (Matrix Science Ltd., London) for mass spectrometry peak identification and quantification. We searched the IPI rat v3.52 (http://www.ebi.ac.uk) with a decoy database search strategy including common contaminants like BSA and proteolytic enzymes, with ±7 ppm and ±0.5 Da mass tolerance at the precursor and fragment levels, respectively. The protein and peptide false-discovery rate for protein identification was set at 0.01. Protein ratios are reported only when two or more peptides were quantitated. Search variables for SILAC were Arg-$^{12}C_6$ and Lys-$^{12}C_6$$^{14}N_2$ (light) or Arg-$^{13}C_6$ and Lys-$^{13}C_6$$^{15}N_2$ (heavy), variable modifications were oxidized methionine and acetylation of protein N termini, whereas only carbamidomethylated cysteines were considered.

In Vitro Kinase Assays

Kinase assays were performed with the ADP-Glo Kinase Assay system (Promega). For the AAK1 kinase assay, 3 ng/μl recombinant AAK1 (Δ-AID) was incubated at room temperature with 300 μM of a custom synthetic AP2M1 peptide substrate (QHQTKEEQSQITSQVT*GQIGWRREGIKYRR), synthesized by the MIT Biopolymers Facility using standard methods, that was based upon the sequence flanking the known AAK1 phosphorylation site (Thr156; marked by asterisk) of rat AP2M1 (Olusanya et al., 2001), and kinase inhibitors at designated concentrations in kinase assay buffer (25 mM Tris, 10 mM MgCl₂, 5 mM DTT, 0.2 units/ml Heparin, 0.1 mg/ml BSA, and 100 μM ATP) for 90 min, and the resulting ADP was detected following the manufacturer's instructions. For GSK3β, 3 ng/μl of kinase was incubated with 10 μM primed phosphopeptide substrate (YRRAAVPPSPSLSRHSSPHQ SpEDEEE) (Ojo et al., 2008). Other conditions were the same as for the AAK1 kinase assay.

Fluorescently Labeled Nrg1

Alexa 594-Nrg1 was prepared using an Alexa 594 protein labeling kit (Invitrogen; A10239) following the vendor's recommended protocol.

Confocal Imaging of ErbB4 and Nrg1 Internalization

PC12-GFP and PC12-ErbB4-GFP cells were incubated with 50 nM K252a for 12 hr, then treated with Alexa 594-Nrg1 (100 ng/ml) for 30 min, and then fixed with 4% paraformaldehyde, permeabilized, and stained with an anti-ErbB4 antibody recognizing the extracellular domain (Lab Vision; MS-270), followed by detection using an anti-mouse IgG-Alexa 488 (Invitrogen; A11001) secondary antibody. Thirty minutes was determined by regular fluorescence microscopy for minimum time allowing detection of internalization. Cells were imaged using confocal microscopy with a 60× objective.

SUPPLEMENTAL INFORMATION

Supplemental Information includes Supplemental Experimental Procedures, four figures, and two tables and can be found with this article online at doi:10.1016/j.chembiol.2011.03.017.

ACKNOWLEDGMENTS

Initiative for Chemical Genetics (contract number N01-CO-12400) and an NIH grant for Genomics Based Drug Discovery-Target ID project (RL1HG004671), administratively linked to RL1CA133834, RL1GM084437, and UL1RR024924. L.K, S.-E.O., C.J.L., and J.M.M. developed biochemical methods, designed, experiments, and analyzed data. J.L.W. provided advice on chemical inhibitors and synthesized analogs of K252a. J.R.D., T.A.L., and X.W. designed, synthesized, and characterized the K252a-based affinity probes. S.-E.O., L.K., and S.A.C. designed, performed, and interpreted the SILAC-target identification studies. S.D.C. provided key reagents and advice for the AAK1 kinase assay, biochemical studies, and data interpretation. D.A.P. designed and performed the K252a-AAK1 computational studies. S.L.S., S.A.C., E.M.S., and S.J.H. provided funding, mentoring, and advised in experimental design and data interpretation. L.K., J.M.M., and S.J.H. prepared the manuscript, which was edited by all authors. The corresponding author (S.J.H.) certifies that all authors have agreed to all the content in the manuscript, including the data as presented. There were no competing financial interests.

REFERENCES

Al-awar, R.S., Ray, J.E., Hecker, K.A., Joseph, S., Huang, J., Shih, C., Brooks, H.B., Spencer, C.D., Watkins, S.A., Schultz, R.M., et al. (2004). Preparation of novel aza-1,7-annulated indoles and their conversion to potent indolocarbazole kinase inhibitors. Bioorg. Med. Chem. Lett. 14, 3925–3928.

Baulida, J., Kraus, M.H., Alimandi, M., Di Fiore, P.P., and Carpenter, G. (1996). All ErbB receptors other than the epidermal growth factor receptor are endocytosis impaired. J. Biol. Chem. 271, 5251–5257.

Berg, M.M., Sternberg, D.W., Parada, L.F., and Chao, M.V. (1992). K-252a inhibits nerve growth factor-induced trk proto-oncogene tyrosine phosphorylation and kinase activity. J. Biol. Chem. 267, 13–16.

Borasio, G.D. (1990). Differential effects of the protein kinase inhibitor K-252a on the in vitro survival of chick embryonic neurons. Neurosci. Lett. 108, 207–212.

Boulton, T.G., Nye, S.H., Robbins, D.J., Ip, N.Y., Radziejewska, E., Morgenbesser, S.D., DePinho, R.A., Panayotatos, N., Cobb, M.H., and Yancopoulos, G.D. (1991). ERKs: a family of protein-serine/threonine kinases that are activated and tyrosine phosphorylated in response to insulin and NGF. Cell 65, 663–675.

Bublil, E.M., and Yarden, Y. (2007). The EGF receptor family: spearheading a merger of signaling and therapeutics. Curr. Opin. Cell Biol. 19, 124–134.

Buonanno, A. (2010). The neuregulin signaling pathway and schizophrenia: from genes to synapses and neural circuits. Brain Res. Bull. 83, 122–131.

Cho, K.O., Skarnes, W.C., Minsk, B., Palmieri, S., Jackson-Grusby, L., and Wagner, J.A. (1989). Nerve growth factor regulates gene expression by several distinct mechanisms. Mol. Cell. Biol. 9, 135–143.

Conner, S.D., and Schmid, S.L. (2002). Identification of an adaptor-associated kinase, AAK1, as a regulator of clathrin-mediated endocytosis. J. Cell Biol. 156, 921–929.

Conner, S.D., Schroter, T., and Schmid, S.L. (2003). AAK1-mediated micro2 phosphorylation is stimulated by assembled clathrin. Traffic 4, 885–890.

Cox, J., and Mann, M. (2008). MaxQuant enables high peptide identification rates, individualized p.p.b.-range mass accuracies and proteome-wide protein quantification. Nat. Biotechnol. 26, 1367–1372.

Debreczeni, J.E., Farkas, L., Harmat, V., Hetenyi, C., Hajdu, I., Zavodszky, P., Kohama, K., and Nyitray, L. (2005). Structural evidence for non-canonical binding of Ca2+ to a canonical EF-hand of a conventional myosin. J. Biol. Chem. 280, 41458–41464.

Fabian, M.A., Biggs, W.H., 3rd, Treiber, D.K., Atteridge, C.E., Azimioara, M.D., Benedetti, M.G., Carter, T.A., Ciceri, P., Edeen, P.T., Floyd, M., et al. (2005). A small molecule-kinase interaction map for clinical kinase inhibitors. Nat. Biotechnol. 23, 329–336.

Falls, D.L. (2003). Neuregulins: functions, forms, and signaling strategies. Exp. Cell Res. 284, 14–30.

Gingrich, D.E., Reddy, D.R., Iqbal, M.A., Singh, J., Aimone, L.D., Angeles, T.S., Albom, M., Yang, S., Ator, M.A., Meyer, S.L., et al. (2003). A new class of potent vascular endothelial growth factor receptor tyrosine kinase inhibitors: structure-activity relationships for a series of 9-alkoxymethyl-12-(3-hydroxy-propyl)indeno[2,1-a]pyrrolo[3,4-c]carbazole-5- ones and the identification of CEP-5214 and its dimethylglycine ester prodrug clinical candidate CEP-7055. J. Med. Chem. 46, 5375–5388.

Glicksman, M.A., Prantner, J.E., Meyer, S.L., Forbes, M.E., Dasgupta, M., Lewis, M.E., and Neff, N. (1993). K-252a and staurosporine promote choline acetyltransferase activity in rat spinal cord cultures. J. Neurochem. 61, 210–221.

Glicksman, M.A., Forbes, M.E., Prantner, J.E., and Neff, N.T. (1995). K-252a promotes survival and choline acetyltransferase activity in striatal and basal forebrain neuronal cultures. J. Neurochem. 64, 1502–1512.

Greene, L.A., and Tischler, A.S. (1976). Establishment of a noradrenergic clonal line of rat adrenal pheochromocytoma cells which respond to nerve growth factor. Proc. Natl. Acad. Sci. USA 73, 2424–2428.

Guy, P.M., Platko, J.V., Cantley, L.C., Cerione, R.A., and Carraway, K.L., 3rd. (1994). Insect cell-expressed p180erbB3 possesses an impaired tyrosine kinase activity. Proc. Natl. Acad. Sci. USA 91, 8132–8136.

Harada, T., Morooka, T., Ogawa, S., and Nishida, E. (2001). ERK induces p35, a neuron-specific activator of Cdk5, through induction of Egr1. Nat. Cell Biol. 3, 453–459.

Hashimoto, S. (1988). K-252a, a potent protein kinase inhibitor, blocks nerve growth factor-induced neurite outgrowth and changes in the phosphorylation of proteins in PC12h cells. J. Cell Biol. 107, 1531–1539.

Heasley, L.E., and Johnson, G.L. (1992). The beta-PDGF receptor induces neuronal differentiation of PC12 cells. Mol. Biol. Cell 3, 545–553.

Henderson, D.M., and Conner, S.D. (2007). A novel AAK1 splice variant functions at multiple steps of the endocytic pathway. Mol. Biol. Cell 18, 2698–2706.

Kaneko, M., Saito, Y., Saito, H., Matsumoto, T., Matsuda, Y., Vaught, J.L., Dionne, C.A., Angeles, T.S., Glicksman, M.A., Neff, N.T., et al. (1997). Neurotrophic 3,9-bis[(alkylthio)methyl]-and-bis(alkoxymethyl)-K-252a derivatives. J. Med. Chem. 40, 1863–1869.

Kaplan, D.R., Martin-Zanca, D., and Parada, L.F. (1991a). Tyrosine phosphorylation and tyrosine kinase activity of the trk proto-oncogene product induced by NGF. Nature 350, 158–160.

Kaplan, D.R., Hempstead, B.L., Martin-Zanca, D., Chao, M.V., and Parada, L.F. (1991b). The trk proto-oncogene product: a signal transducing receptor for nerve growth factor. Science 252, 554–558.

Karaman, M.W., Herrgard, S., Treiber, D.K., Gallant, P., Atteridge, C.E., Campbell, B.T., Chan, K.W., Ciceri, P., Davis, M.I., Edeen, P.T., et al. (2008). A quantitative analysis of kinase inhibitor selectivity. Nat. Biotechnol. 26, 127–132.

Kase, H., Iwahashi, K., and Matsuda, Y. (1986). K-252a, a potent inhibitor of protein kinase C from microbial origin. J. Antibiot. (Tokyo) 39, 1059–1065.

Knusel, B., and Hefti, F. (1992). K-252 compounds: modulators of neurotrophin signal transduction. J. Neurochem. 59, 1987–1996.

Koizumi, S., Contreras, M.L., Matsuda, Y., Hama, T., Lazarovici, P., and Guroff, G. (1988). K-252a: a specific inhibitor of the action of nerve growth factor on PC 12 cells. J. Neurosci. 8, 715–721.

Kuai, L., Wang, X., Madison, J.M., Schreiber, S.L., Scolnick, E.M., and Haggarty, S.J. (2010). Chemical genetics identifies small-molecule modulators of neuritogenesis involving neuregulin-1/ErbB4 signaling. ACS Chem. Neurosci. 1, 325–342.

Kuo, G.H., Prouty, C., DeAngelis, A., Shen, L., O'Neill, D.J., Shah, C., Connolly, P.J., Murray, W.V., Conway, B.R., Cheung, P., et al. (2003). Synthesis and discovery of macrocyclic polyoxygenated bis-7-azaindolylmaleimides as a novel series of potent and highly selective glycogen synthase kinase-3beta inhibitors. J. Med. Chem. 46, 4021–4031.

Latourelle, J.C., Pankratz, N., Dumitriu, A., Wilk, J.B., Goldwurm, S., Pezzoli, G., Mariani, C.B., DeStefano, A.L., Halter, C., Gusella, J.F., et al. (2009). Genomewide association study for onset age in Parkinson disease. BMC Med. Genet. 10, 98.

Lazarovici, P., Levi, B.Z., Lelkes, P.I., Koizumi, S., Fujita, K., Matsuda, Y., Ozato, K., and Guroff, G. (1989). K-252a inhibits the increase in c-fos transcription and the increase in intracellular calcium produced by nerve growth factor in PC12 cells. J. Neurosci. Res. 23, 1–8.

Liu, Y., Tao, Y.M., Woo, R.S., Xiong, W.C., and Mei, L. (2007). Stimulated ErbB4 internalization is necessary for neuregulin signaling in neurons. Biochem. Biophys. Res. Commun. 354, 505–510.

Longart, M., Chatani-Hinze, M., Gonzalez, C.M., Vullhorst, D., and Buonanno, A. (2007). Regulation of ErbB-4 endocytosis by neuregulin in GABAergic hippocampal interneurons. Brain Res. Bull. 73, 210–219.

Maroney, A.C., Lipfert, L., Forbes, M.E., Glicksman, M.A., Neff, N.T., Siman, R., and Dionne, C.A. (1995). K-252a induces tyrosine phosphorylation of the focal adhesion kinase and neurite outgrowth in human neuroblastoma SH-SY5Y cells. J. Neurochem. 64, 540–549.

Mei, L., and Xiong, W.C. (2008). Neuregulin 1 in neural development, synaptic plasticity and schizophrenia. Nat. Rev. Neurosci. 9, 437–452.

Miyasaka, T., Chao, M.V., Sherline, P., and Saltiel, A.R. (1990). Nerve growth factor stimulates a protein kinase in PC-12 cells that phosphorylates microtubule-associated protein-2. J. Biol. Chem. 265, 4730–4735.

Moffat, J., Grueneberg, D.A., Yang, X., Kim, S.Y., Kloepfer, A.M., Hinkle, G., Piqani, B., Eisenhaure, T.M., Luo, B., Grenier, J.K., et al. (2006). A lentiviral RNAi library for human and mouse genes applied to an arrayed viral high-content screen. Cell 124, 1283–1298.

Morotti, A., Mila, S., Accornero, P., Tagliabue, E., and Ponzetto, C. (2002). K252a inhibits the oncogenic properties of Met, the HGF receptor. Oncogene 21, 4885–4893.

Murakata, C., Kaneko, M., Gessner, G., Angeles, T.S., Ator, M.A., O'Kane, T.M., McKenna, B.A., Thomas, B.A., Mathiasen, J.R., Saporito, M.S., et al. (2002). Mixed lineage kinase activity of indolocarbazole analogues. Bioorg. Med. Chem. Lett. 12, 147–150.

Nye, S.H., Squinto, S.P., Glass, D.J., Stitt, T.N., Hantzopoulos, P., Macchi, M.J., Lindsay, N.S., Ip, N.Y., and Yancopoulos, G.D. (1992). K-252a and staurosporine selectively block autophosphorylation of neurotrophin receptors and neurotrophin-mediated responses. Mol. Biol. Cell 3, 677–686.

Ojo, K.K., Gillespie, J.R., Riechers, A.J., Napuli, A.J., Verlinde, C.L., Buckner, F.S., Gelb, M.H., Domostoj, M.M., Wells, S.J., Scheer, A., et al. (2008). Glycogen synthase kinase 3 is a potential drug target for African trypanosomiasis therapy. Antimicrob. Agents Chemother. 52, 3710–3717.

Olusanya, O., Andrews, P.D., Swedlow, J.R., and Smythe, E. (2001). Phosphorylation of threonine 156 of the mu2 subunit of the AP2 complex is essential for endocytosis in vitro and in vivo. Curr. Biol. 11, 896–900.

Ong, S.E., and Mann, M. (2006). A practical recipe for stable isotope labeling by amino acids in cell culture (SILAC). Nat. Protoc. 1, 2650–2660.

Ong, S.E., Blagoev, B., Kratchmarova, I., Kristensen, D.B., Steen, H., Pandey, A., and Mann, M. (2002). Stable isotope labeling by amino acids in cell culture, SILAC, as a simple and accurate approach to expression proteomics. Mol. Cell. Proteomics 1, 376–386.

Ong, S.E., Schenone, M., Margolin, A.A., Li, X., Do, K., Doud, M.K., Mani, D.R., Kuai, L., Wang, X., Wood, J.L., et al. (2009). Identifying the proteins to which small-molecule probes and drugs bind in cells. Proc. Natl. Acad. Sci. USA 106, 4617–4622.

Pearlman, D. (1998). Free energy calculations: methods and applications. In The Encyclopedia of Computational Chemistry, B.G. Rao, ed. (New York: John Wiley & Sons), pp. 1036–1061.

Pollack, S., Young, L., Bilsland, J., Wilkie, N., Ellis, S., Hefti, F., Broughton, H., and Harper, S. (1999). The staurosporine-like compound L-753,000 (NB-506) potentiates the neurotrophic effects of neurotrophin-3 by acting selectively at the TrkA receptor. Mol. Pharmacol. 56, 185–195.

Rappsilber, J., Mann, M., and Ishihama, Y. (2007). Protocol for micro-purification, enrichment, pre-fractionation and storage of peptides for proteomics using StageTips. Nat. Protoc. 2, 1896–1906.

Ricotta, D., Conner, S.D., Schmid, S.L., von Figura, K., and Honing, S. (2002). Phosphorylation of the AP2 mu subunit by AAK1 mediates high affinity binding to membrane protein sorting signals. J. Cell Biol. 156, 791–795.

Roux, P.P., Dorval, G., Boudreau, M., Angers-Loustau, A., Morris, S.J., Makkerh, J., and Barker, P.A. (2002). K252a and CEP1347 are neuroprotective compounds that inhibit mixed-lineage kinase-3 and induce activation of Akt and ERK. J. Biol. Chem. 277, 49473–49480.

Ruegg, U.T., and Burgess, G.M. (1989). Staurosporine, K-252 and UCN-01: potent but nonspecific inhibitors of protein kinases. Trends Pharmacol. Sci. 10, 218–220.

Sanchez, C., Mendez, C., and Salas, J.A. (2006). Indolocarbazole natural products: occurrence, biosynthesis, and biological activity. Nat. Prod. Rep. 23, 1007–1045.

Schiering, N., Knapp, S., Marconi, M., Flocco, M.M., Cui, J., Perego, R., Rusconi, L., and Cristiani, C. (2003). Crystal structure of the tyrosine kinase domain of the hepatocyte growth factor receptor c-Met and its complex with the microbial alkaloid K-252a. Proc. Natl. Acad. Sci. USA 100, 12654–12659.

Smith, D.S., King, C.S., Pearson, E., Gittinger, C.K., and Landreth, G.E. (1989). Selective inhibition of nerve growth factor-stimulated protein kinases by K-252a and 5′-S-methyladenosine in PC12 cells. J. Neurochem. 53, 800–806.

Smythe, E., and Ayscough, K.R. (2003). The Ark1/Prk1 family of protein kinases. Regulators of endocytosis and the actin skeleton. EMBO Rep. 4, 246–251.

Sorkin, A., and Goh, L.K. (2008). Endocytosis and intracellular trafficking of ErbBs. Exp. Cell Res. 314, 3093–3106.

Stockwell, B.R. (2000). Chemical genetics: ligand-based discovery of gene function. Nat. Rev. 1, 116–125.

Sundvall, M., Korhonen, A., Paatero, I., Gaudio, E., Melino, G., Croce, C.M., Aqeilan, R.I., and Elenius, K. (2008). Isoform-specific monoubiquitination, endocytosis, and degradation of alternatively spliced ErbB4 isoforms. Proc. Natl. Acad. Sci. USA 105, 4162–4167.

Tapley, P., Lamballe, F., and Barbacid, M. (1992). K252a is a selective inhibitor of the tyrosine protein kinase activity of the trk family of oncogenes and neurotrophin receptors. Oncogene 7, 371–381.

Traverse, S., Gomez, N., Paterson, H., Marshall, C., and Cohen, P. (1992). Sustained activation of the mitogen-activated protein (MAP) kinase cascade may be required for differentiation of PC12 cells. Comparison of the effects of nerve growth factor and epidermal growth factor. Biochem. J. 288, 351–355.

Tzahar, E., Levkowitz, G., Karunagaran, D., Yi, L., Peles, E., Lavi, S., Chang, D., Liu, N., Yayon, A., Wen, D., et al. (1994). ErbB-3 and ErbB-4 function as the respective low and high affinity receptors of all Neu differentiation factor/heregulin isoforms. J. Biol. Chem. 269, 25226–25233.

Wang, X., Imber, B.S., and Schreiber, S.L. (2008). Small-molecule reagents for cellular pull-down experiments. Bioconjug. Chem. 19, 585–587.

Wen, L., Lu, Y.S., Zhu, X.H., Li, X.M., Woo, R.S., Chen, Y.J., Yin, D.M., Lai, C., Terry, A.V., Jr., Vazdarjanova, A., et al. (2010). Neuregulin 1 regulates pyramidal neuron activity via ErbB4 in parvalbumin-positive interneurons. Proc. Natl. Acad. Sci. USA 107, 1211–1216.

Woo, R.S., Li, X.M., Tao, Y., Carpenter-Hyland, E., Huang, Y.Z., Weber, J., Neiswender, H., Dong, X.P., Wu, J., Gassmann, M., et al. (2007). Neuregulin-1 enhances depolarization-induced GABA release. Neuron 54, 599–610.

Yang, X.L., Huang, Y.Z., Xiong, W.C., and Mei, L. (2005). Neuregulin-induced expression of the acetylcholine receptor requires endocytosis of ErbB receptors. Mol. Cell. Neurosci. 28, 335–346.

Zhang, H.C., Derian, C.K., McComsey, D.F., White, K.B., Ye, H., Hecker, L.R., Li, J., Addo, M.F., Croll, D., Eckardt, A.J., et al. (2005). Novel indolylindazolylmaleimides as inhibitors of protein kinase C-beta: synthesis, biological activity, and cardiovascular safety. J. Med. Chem. 48, 1725–1728.